Topological carbon allotropes: knotted molecules, carbon-nano-chain, chainmails, and Hopfene

Shinichi Saito[1,*] **and Isao Tomita**[2]

[1]Sustainable Electronic Technologies Research Group, Electronics and Computer Science, Faculty of Engineering and Physical Sciences, University of Southampton, SO17 1BJ, UK.
[2]Department of Electrical and Computer Engineering, National Institute of Technology, Gifu College, 2236-2 Kamimakuwa, Motosu, Gifu 501-0495, Japan.
[*]s.saito@soton.ac.uk, Present address: Center for Exploratory Research Laboratory, Research & Development Group, Hitachi, Ltd. Tokyo 185-8601, Japan.

ABSTRACT

Carbon allotropes such as diamond, nano-tube, Fullerene, and Graphene were discovered and revolutionised material sciences. These structures have unique translational and rotational symmetries, described by a crystallographic group theory, and the atoms are arranged at specific rigid positions in 3-dimensional (D) space. Regardless of these exotic molecular structures, the structures of materials are topologically trivial in a mathematical sense, that their bonds are connected without a link nor a knot. These days, the progress on the synthetic chemistry is significant to make various topologically non-trivial molecular structures. Topological molecules ($0D$) including Trefoil knots, a Hopf-link, a Möbius strip, and Borromean rings, were already realised. However, their potentially exotic electronic properties have not been sufficiently explored. Here, we propose a new 3D carbon allotrope, named Hopfene, which has periodic arrays of Hopf-links to knit horizontal Graphene sheets into vertical ones without connecting by σ bonds. We conducted an *ab inito* band structure calculation using a Density-Functional-Theory (DFT) for Hopfene, and found that it is well-described by a tight-binding model. We confirmed the original Dirac points of $2D$ Graphene were topologically protected upon the introduction of the Hopf links, and low-energy excitations are described by $1D$, $2D$, and $3D$ gapless Fermions.

Introduction

Mass of an elementary particle is related to a broken symmetry of a vacuum, and the energy-momentum relationship is linked to the symmetries of the vacuum[1]. In solid state physics, materials with certain symmetries can be designed, and carbon allotropes are useful due to their richness in families with various translational and rotational symmetries of crystals, such as a cage like a Fullerene[2], a tube called a carbon-nano-tube[3,4], and a sheet including a Graphene[5–7]. However, these materials have topologically trivial crystal structures without having a link nor a knot. On the other hand, a lot of synthetic materials have non-trivial topological configurations, for example polymers[8–10], macromolecules[11–14], and proteins[15].

Research areas on topology are spanning from pure mathematics[16–19], physics[20–25], to chemistry[11–15]. Mathematicians could even classify the shape of our universe[18] and proved the Poincaré conjecture successfully[19]. In condensed-matter physics, vortex and anti-vortex pairs in superconductors exhibit unusual topological phase transitions due to their binding and dissociations across the transition temperature[20,21]. More recently, a topological insulator was proposed theoretically[23] and discovered experimentally[24], which showed insulating character in the bulk regardless of its conducting surface. In these materials, quantum states exhibit inherent topological nature[20,21,23] upon the appropriate choice of materials[24]. Nontrivial topological structures themselves were also chemically synthesised[8–15].

Regardless of these advanced chemistry to synthesise topologically non-trivial materials[8–15], the corresponding electronic structures of topological carbon allotropes are not examined in great detail. The chemical structures are apparent in real space, while the electronic structures can be described in momentum space as band diagrams[26]. From a quantum-mechanical point of views, we expect a duality relationship between real space and momentum space. Our hypothesis is to obtain a non-trivial band structure from a chemically non-trivial material. Here, a non-trivial band structure means the existence of a massless dispersion, similar to be described by Dirac Fermions[4,27,28], which can be considered to be generated by magnetic monopoles. A lot of efforts are being made to find $3D$ Dirac fermions[29–31], but most of major progress on topological electronic materials in the last decade were achieved by investigating band structures of topologically trivial crystalline structures[31–35], as evidenced by the title of the paper[33], as an example, claiming *unconventional quasiparticles in conventional crystals*. We have no objection of these state-of-the-art activities in physics and we have no intention to challenge this paradigm. Nevertheless, we believe it is worth for considering chemically non-trivial crystal structures for the possible emergence of non-trivial electronic structures. It

would be more straightforward to find topologically non-trivial band structures, with the helps of structures, such that it is less exciting for physicists. However, we think we do not have to restrict ourselves to investigate conventional crystals, if the purpose is innovation to find novel band structures. If we restricted ourselves to investigate materials, which have perfect crystalline structures only, Graphene would not be discovered, since the absence of the long-range order in $2D$ was rather rigorously proved theoretically by Mermin-Wager[36] and Hohenberg[37]. It is the existence of a ripple[28], which stabilises Graphene at finite temperature, such that strictly rigid long-range order as a crystal is absent. Another examples of a successful hypothetical model is found in strongly correlated electronic systems[38,39]. It was proposed to investigate a tight-binding Hubbard model in an infinite dimensional ($D = \infty$) hypercubic lattice[38], which cannot exist in nature. However, the proposed scaling law[38] of the tight-binding hopping parameter as $t \to t^*/\sqrt{D}$ resulted in a simplified Gaussian density of state, while keeping non-trivial nature of many-body problems, leading to the great success as a dynamical mean-field theory[39].

Structures

Topological molecules ($0D$)

We have used Chem3D, a molecular editor, for molecular-mechanical simulations, using classical mechanics with empirical parameters[40]. We considered many topological molecules (Figs. 1-2, Supplementary Videos 1 and 2). The most direct applications of topological materials would be Nano-Electro-Mechanical-Systems (NEMS)[41], towards developing a molecular motor and associated advanced chemical technologies[11–15,22]. Figure 1a shows an ultimate example of trapped 1 benzene molecule using a straight-chain alkane of 1D atomistic carbon atoms connected to a Graphene sheet (Supplementary Video 1). It is technologically accessible to make such a molecular motor by combining patterning technologies of a free-standing Graphene sheet by ion or electron beam irradiations and growth technologies such as Chemical-Vapour-Deposition[42]. The combination is very important to construct a topologically complex structures, because we must close the bond (in this case, the benzene ring) without affecting the other bonds (straight-chain). Obviously, larger molecules and wider chain will be more suitable to construct a practical NEMS device.

In order to realise directional rotation of a molecular motor, it is important to control chirality of a molecule. The most simplest nontrivial knot is the Trefoil knot, which has a chiral counter part (Fig. 1c). The left (right) Trefoil knot has always left (right) spiral circulation as climbing up the strand (Supplementary Video 2). In other words, handedness is memorised in the molecule, which will be useful for applications in molecular memories and polarisation rotators. Recently, all-benzene based catenane molecules of both left and right handed trefoil knots and and a Hopf-link were successfully achieved[43]. A completely circular molecular ring was also synthesised[44].

It is not possible to memorise the handedness solely by twisting a 1D carbon ring to the left or the right, since it merely change the geometry without changing the topology (Fig. 1b). In order to memorise the handedness, we need to lock the status of the twisted ring, by inserting the other molecule into the ring and close the bond. Then, we can make left and right topological molecules of Whitehead-links, whose handedness will be protected against the deformations of molecules as far as the bonds are sustained.

The situation is slightly changed, if we employ a Graphene nano-ribbon[45]. Even if it consists of just several benzene rings, the ring will define a $2D$ plane to confine the ribbon so that it is different from a pure 1D chain. As a result, the Möbius strip[22,46,47] can memorise the handedness whether the Graphene nano-ribbons were twisted to the left or the right before bonding without using another Graphene nano-ribbon (Fig. 1d). Moreover, the number of twisted rotations is also a topologically protected valuable as a winding number, which is also robust against the deformation. We also considered even more complex structure such as Borromean rings[48,49] (Fig. 1e). To our surprise, the converged structure is rather beautiful with a proper symmetry upon exchanging rings, which was energetically favourable rather than keeping random deformations.

Besides knots, the simplest nontrivial link is the Hopf-link[12,14–16] (Figs. 2a-2f). We found a benzene ring can sustain its σ bonds, while allowing another benzene ring to penetrate without making a proper σ bond. The benzene ring can move freely without changing the topology of the Hopf-link, which will be a huge advantage to make flexible devices. However, the bond lengths of the benzene-based Hopf-link are significantly expanded, so that the high tensile strains of the order of 20% are accumulated (Fig. 2a). Therefore, it is not possible to introduce 2 benzene rings into 1 ring (Fig. 2b and Supplementary Video 2). This will certainly limit the use of the benzene-based Hopf-link towards the construction of the $1D$ chain.

However, if we use 2 connected benzene rings (Naphthalene, $C_{10}H_8$), we can overcome this problem, since the insertion of just 1 benzene ring into the Naphthalene is enough for extending the length of the $1D$ Carbon-Nano-Chain (Figs. 2c and 3). We also considered to open-up one of the benzene ring of Naphthalene (Fig. 1 b), which corresponds to use a larger ring (Cyclodecapentaene, $C_{10}H_{10}$) for the Hopf-link (Fig. 2d), whose bonds are significantly relaxed. In the larger ring, we could introduce as many as 4 rings (Fig. 2e), so that we can also construct the $2D$ 4-in-1 Chainmail (Fig. 3c) in addition to a standard Chain (Supplementary Fig. 3b).

Topological Chains (1D) and Chainmail (2D)

For the simulations of the rolled Chains (Figs. 3-4) and Chainmail (Fig. 3), we have gradually changed the initial coordination of atoms. If we changed the initial condition significantly different from the previously converged geometries, Hopf-links were completely broken and the structures were topologically changed. This will also happen in the real situation, where the external force exceeded the threshold enough to break one of the σ bonds for the Hopf-links. Conversely, the proposed Chains and Chainmail will be topologically robust as far as the σ bonds are maintained. Thus, we expect a topologically flexible material, which would be as flexible as a rubber, while it is very stiff as hard as or even harder than a diamond due to its sp^2 nature of the rings.

The unique features of these Chains and Chainmail are their flexibility with the rigidity ensured by the σ bonds (Fig. 3 and Supplementary Video 3). Our Chains can be aligned to be straight-lines or to be rolled-up without breaking the topological links (Fig. 4). The lengths can be changed to be several times, while it will be difficult to change the lengths of Carbon-Nano-Tubes[3] due to its strong rigidity. The σ bonds using sp^2 orbitals are considered to be even stronger than sp^3 bonds of diamond, so that our chains will be much stronger than flexible polyacetylene[50]. It is interesting to consider a similarity of our proposed Chain to a macroscopic metallic chain and chainmail, against the Fullerene[2] to a football. We think that it would not be mere coincidence that we came up to the same structure that the human race is already using for a long time. The idea behind the football shape would be its high spherical symmetry. It is the compatibility of flexibility with its rigidity why people made a chain, by introducing the Hopf-links[16] even without being aware of mathematical rigidity. The argument would also be true in the molecular level (Fig. 4).

We have simulated various configurations of Chains by changing the boundary conditions. For example, by introducing a twisted boundary conditions between one end of the chain to the other for the 1D Hopf-linked Chain, we could introduce a global kink as a form of a soliton, which is a topologically protected excitation (Fig. 4). Upon rotating twice, we found the chain was broken due to the high tensile strains accumulated in the Chain (Fig. 4e).

The chain can memorise the global winding number and the chirality (the left or the right rotation) upon twisting the Chain (Fig. 4). This situation is completely different from a 1D atomic chain like a polyacetylene (Fig. 4f), due to its rotational symmetry. One might think that polyacetylene would be more tolerant against the rotational disturbance, but no restoration force will work to prevent the rotation. On the other hand, the Hopf-linked chain can accumulate the global strain and the restoration force will be generated to protect itself against the structural deformation. This would be related to the reason why DNA with a double-stranded spiral structure was naturally selected due to its stronger tolerance in a competitive environment.

The geometrical coordinates of straight and rolled Carbon-Nano-Chains are apparently different, while both structures are topologically equivalent. Therefore, we can regard these chains as possessing *Topological-Long-Range-Order (TLRO)* even without having translational nor rotational symmetries. We can construct whole new varieties of materials with TLRO, as *topological materials*, which will not be categorised as a conventional crystal nor a completely-randomised amorphous material. Chains and Chainmail are clear examples of topological materials.

Topological Crystal: Hopfene (3D)

We have considered various structures, such as topological molecules (0D, Figs. 1-2, Supplementary Videos 1-2), 1D Carbon-Nano-Chains (CNC, Figs. 3 and 4, Supplementary Video 3), and 2D Chainmails (Fig. 3). The concept of *Topological-Long-Range-Order (TLRO)* is also applicable to a 3D structure, and the idea of a *topological crystal*[8–10] would be as exciting as a time crystal[51]. We have conceived to the idea of a new 3D carbon allotrope by considering nested structures with stacked Graphene sheets both vertically and horizontally, while the intersections of these sheets are made of Hopf-links (Figs. 5-8, Supplementary Figs. 1-6, and Supplementary Video 4). To our surprise, the optimised structures have almost perfect translational symmetries, so that these will be realised as a conventional single crystal.

We proposed to call this new structure, as *Hopfene*[52,53], named after a mathematician, Heinz Hopf, because of the importance of Hopf-links[16] for this crystal. Here, we describe the details of physical and electronic structures of Hopfene. Similar to Carbon-Nano-Tubes[3], which has a family of allotropes depending on how to roll-up a Graphene sheet, Hopfene also has a family depending on how to insert Graphene sheets (Supplementary Figs. 1-6, and Supplementary Video 4). Graphene sheets were inserted perpendicular to the other stacks, and it was important to align the directions of the zig-zag edges in parallel to match the periodicity of the Graphene lattice (Supplementary Fig. 2). Let's assume that we inserted the first sheet to the bottom available slot, labelled as slot 0 (Supplementary Fig. 2). If we insert next sheets into the most adjacent available slot, slot 1, for both horizontal (x) and vertical (y) directions, the structure is called as (1,1) Hopfene (Figs. 5a, 5d, and Supplementary Fig. 2). In this case, the adjacent stacks are half-lattice constant shifted ($c/2$) along zig-zag edge (z) direction, so that the stack is called as AB-stack. On the other hand, if we insert Graphene sheets into slot 2, while making the slot 1 empty, the structure is called as (2,2) Hopfene (Figs. 5b, 5e, and Supplementary Fig. 2). In this case, the nearest adjacent sheets are aligned so that the stack is called as AA-stack. We considered more complicated insertions, such as the insertion into slot 1 for x-direction, while the insertion along y-direction is from slot 2, whose structure is (1,2) Hopfene (Figs. 5c, 5f,

and Supplementary Fig. 3). In general, there exists (n,m) Hopfene, where n and m are integers to describe the insertion of Graphene sheets, and if n and m are odd (even), the sheets are AB (AA) stack. If $n = m$, the Hopfene structure is tetragonal with the lattice constants $a = b \neq c$, while it is orthogonal ($a \neq b \neq c$) for $n \neq m$. Therefore, we can recognise rectangular holes if we see the structure from the bottom (Fig. 5). These holes would allow carrier doping by intercalation, which may lead superconductivity similar to alkali-metal doped Fullerenes[54]. If n and m are large, the size of the hole will be large, so that the Graphene sheets and the crystal itself can be deformed substantially, breaking the translational symmetry. It is also expected that the actual experimental structures would be different due to the huge strains accumulated in rings, as theoretically predicted in a highly-strained Graphene, which stabilised to be a dimerised Kekulé-like structure[55]. Even in that case, TLRO would be kept as far as σ bonds survived to keep Hopf-links.

Hopfene is made by stacking two-dimensional ($2D$) honeycomb lattices, Graphene[5–7] sheets, both vertically and horizontally with arrays of Hopf-links at intersections (Supplementary Figs. 1-6). The Graphene sheets are aligned parallel to the direction along zig-zag edges and perpendicular to the arm-chair edges. In contrast to Carbon-Nano-Tubes (CNTs), for which the structures were categorised by the way of rolling up a Graphene sheet, Hopfene is characterised by the way of inserting Graphene sheets. In the example of Fig. 5, available slots for Graphene sheets are occupied alternatively by AA-stacking, which we refer to as (2,2)-Hopfene. The crystal is tetragonal with the lattice constants of $a = b = 3a_0$ within the $x-y$ plane and $c = \sqrt{3}a_0$ along z (Figs. 5 (d) and 5 (e)) at the bond length of a_0.

Hopfene was made by preparing AA-stacked Graphene sheets, separated by the distance of the lattice constant of a Graphene, which is the adjacent distance between the sides of the ring (Supplementary Figs. 3 and 4). Depending on the targeted stacking, described by (n,m) where n and m are integers for the available slots along horizontal (x) and vertical (y) directions, the number of inserted Graphene sheets and separations were adjusted. We have prepared the Graphene sheets by hands using the GUI (Graphical User Interface) of the software, so that the position and the distance were not perfect. This uncertainty resulted in the formation of *topological defects* in the final structure (Supplementary Fig. 1), but we kept as it is to highlight new types of defects without broken bonds. Then, we optimised the structure relying on the algorithm of the software to minimise the energy. After the optimisation, for (1,1) Hopfene, AB-stack was automatically chosen for both x and y directions by shifting the Graphene sheets with the amount of the half of the lattice constant along z direction, regardless of the initial condition of AA-stack. Here, please note that AB-stack of Hopfene is different from AB-stack of Graphite. AB-stack of Hopfene means the parallel-shift of the Graphene sheet along the zig-zag edge (Supplementary Fig. 2), while AB-stack of Graphite is the parallel-shift along the arm-chair edge, so that the directions are perpendicular to that of Hopfene. The process of the convergence of the structure would be similar to the growth process in experiments for the future, so that we have recorded as a video (Supplementary Video 4).

We have examined the stability of (2,2)-Hopfene by a first principle calculation based on a Density-Functional-Theory (DFT) using Quantum Espresso[56], as shown in Fig. 9. The symmetry of the crystal, required for the *ab-initio* calculation, is $P4_2$ (space group number 77). We confirmed the existence of the energy minimum as a function of the volume, which suggests that (2,2)-Hopfene is thermodynamically stable. The calculated energy and the curve are similar to those calculated for Graphite and diamonds[57]. We admit that simple energetic calculations are not sufficient enough to prove the existence of Hopfene as a stable material. Nevertheless, the lattice site of Hopfene does not have to be made of 1 carbon atom, and it could be made of a molecule. In fact, similar materials with topologically non-trivial crystal structures were experimentally found in polymers[8–10]. The interwoven honeycomb lattice[8] of $[Cu_2(C_4H_4N_2)_3(SiF_6)]_\infty$ is very similar to Hopfene with a slightly different crystal symmetry[58] of $I4/mcm$ due to ligands. For these soft materials, the rigid translational symmetries can be broken due to weak Hopf-links, while the topological structures are maintained as long as strong bonds are not broken. The effective tight-binding Hamiltonian for these polymers would be similar to that investigated in this study, if the molecular element is regarded as a lattice site.

Results

Band Structure

In order to obtain the analytic model for the band structure, we have employed a tight-binding Hamiltonian for (2,2)-Hopfene as follows:

$$\hat{H} = \sum_{\mathbf{k}\sigma} \hat{\psi}^\dagger_{\mathbf{k}\sigma} \begin{pmatrix} \mathscr{H}_{\mathrm{G}}(h_{\mathrm{AB}}) & \mathscr{H}_{\mathrm{H}} \\ \mathscr{H}^\dagger_{\mathrm{H}} & \mathscr{H}_{\mathrm{G}}(h_{\mathrm{CD}}) \end{pmatrix} \hat{\psi}_{\mathbf{k}\sigma}, \tag{1}$$

where $\hat{\psi}^\dagger_{\mathbf{k}\sigma} = \left(a^\dagger_{\mathbf{k}\sigma}, b^\dagger_{\mathbf{k}\sigma}, c^\dagger_{\mathbf{k}\sigma}, d^\dagger_{\mathbf{k}\sigma}\right)$ and $\hat{\psi}_{\mathbf{k}\sigma}$ are creation and annihilation operators for electrons with the momentum $\mathbf{k}$ (in units $2\pi(a^{-1}, a^{-1}, c^{-1})$) and the spin σ in A-D sublattices. The matrix components in Graphene sheets are

$$\mathscr{H}_{\mathrm{G}}(h) = \begin{pmatrix} 0 & h \\ h^* & 0 \end{pmatrix}$$

with $h_{\rm AB} = -t_{\rm G}(e^{ik_x a/3} + 2e^{-ik_x a/6}\cos(k_z c/2))$ and $h_{\rm CD} = -t_{\rm G}(e^{ik_y a/3} + 2e^{-ik_y a/6}\cos(k_z c/2))$. We assumed the nearest neighbour hopping energy of $t_{\rm G} = 2.8$ eV within Graphene sheets[4,28]. The components for Hopf-links are described by the following 2×2 matrix

$$\mathscr{H}_{\rm H} = -t_{\rm H}\left(\phi^{\dagger}_{-\frac{k_x}{6}}\phi_{\frac{k_y}{3}} + \phi^{\dagger}_{\frac{k_x}{3}}\phi_{-\frac{k_y}{6}} + 2\cos(\tfrac{k_z c}{2})\phi^{\dagger}_{-\frac{k_x}{6}}\phi_{-\frac{k_y}{6}}\right),$$

with $\phi_k = \left(e^{ika}, e^{-ika}\right)$. We also assumed the nearest neighbour hopping energy of $t_{\rm G}$ through the Hopf link. By inserting $\mathscr{H}_{\rm G}$ and $\mathscr{H}_{\rm H}$ into $\hat{H}$, we obtain the tight-binding Hamiltonian.

We confirmed that energy dispersions are the same as those established for Dirac Fermions in Graphene[4,27,28] in the limit of the absence of the Hopf-link transfer, $t_{\rm H} \to 0$ for both AB and CD Graphene sheets. It is important, however, to note that the dispersions are flat along directions perpendicular to Graphene sheets, because the electrons are confined within the Graphene sheets without the Hopf-links.

In this paper, we have considered only nearest neighbour hopping for the simplest structure of AA-stacked (2,2)-Hopfene among the family of (m,n)-Hopfene as the first analytic step. In principle, any band structures can be described by a tight-binding Hamiltonian, since the Wannier wavefunction forms a complete orthogonal basis, if we consider all higher-order hopping matrix elements, t_{ij}[59], where i and j describe the lattice sites. t_{ij} is approximately proportional to the overlap integral, such that it decreases exponentially against the distance between i-th and j-th atomic sites. In Graphene, it is established that the limitation to the nearest neighbour hopping is a good approximation to describe the low energy excitation near the Dirac points[4,28] The nearest neighbour distance in a Graphene sheet is a_0, while the next nearest neighbour distance is $\sqrt{3}a_0 \approx 1.7a_0$. On the other hand, the nearest and the next neighbour distance of a Hopf link are $\sqrt{5}a_0/2 \approx 1.1a_0$ and $\sqrt{17}a_0/2 \approx 2.1a_0$, respectively. Therefore, we think that we can safely neglect the nearest neighbour hopping through Hopf-links. The impact of the spin-orbit interaction is also weak.

The Hamiltonian at each k is described by a 4×4 matrix, such that the system has an SU(2) $\otimes$ SU(2) symmetry to describe electron transfers within and between Graphene sheets. We have diagonalised the matrix to obtain the band dispersions, $E_1(\mathbf{k})$-$E_4(\mathbf{k})$, which were labelled from 1 to 4, assigned from the lower energies (Figs. 10-11). By the comparison with the the first principle DFT calculation[40] (Fig. 12), we obtained $t_{\rm H} \approx 1.5 \pm 0.5$ eV. The tight-binding results could reproduce important features such as gapless points and flat-band structures near the Fermi energy, $E_{\rm F}$=1.1 eV for non-doped Hopfene, and the tight-binding model is suitable for the low-energy excitation of Hopfene.

In Graphene, Dirac points are located at $K = (0, -2/3)$ and $K' = (0, +2/3)$, and there are 4 equivalent points at $(\pm 1, \pm 1/3)$ due to the symmetry of the $2D$ honeycomb lattice[4]. In Hopfene, on the other hand, these 6 gapless points for horizontal and vertical Graphene sheets are not equivalent, because these are located in different planes within the first Brillouin zone. Consequently, there are 10 gapless points in Hopfene with $t_{\rm H} = 0$ located at $(\pm 1, 0, \pm 1/3)$, $(0, \pm 1, \pm 1/3)$, and $(0, 0, \pm 2/3)$. In particular, the last points of $(0, 0, \pm 2/3)$ are degenerate, because these originate from both horizontal and vertical Graphene sheets. In the presence of $t_{\rm H} \neq 0$, the gapless points will be shifted in $\mathbf{k}$-space, and the slope of the dispersion will be changed, but the essential topological feature will remain unchanged.

The other interesting feature of the band diagram in Hopfene is the emergence of the flat-bands (Fig. 10). At $t_{\rm H} = 0$, bands will not be dispersive along the direction perpendicular to the Graphene sheets (Fig. 10 (a)), and therefore the gapless points will become nodal lines (Fig. 11)[31]. Both gapless points and nodal lines are topologically protected, so that they cannot disappear by adiabatic turn-on of $t_{\rm H}$ (Fig. 10 (b)), unless gapless points or nodal lines with opposite geometrical winding numbers would be merged, simultaneously, leading to the destruction of apparent monopoles with opposite magnetic charge.

It was not possible to obtain an analytic solution of $\hat{H}$ in general, regardless of its simplicity. Therefore, we have checked the weak coupling limit, $t_{\rm H} \to 0$ at $(0, 0, 2/3)$, where we obtain

$$\begin{aligned}
\mathscr{H}_{\rm G}(h_{\rm AB}) &\approx \hbar v_{\rm G}(\sigma_1 \tilde{k}_z + \sigma_2 k_x) \\
\mathscr{H}_{\rm G}(h_{\rm CD}) &\approx \hbar v_{\rm G}(\sigma_1 \tilde{k}_z + \sigma_2 k_y) \\
\mathscr{H}_{\rm H} &\approx (-t_{\rm H} + \hbar\tilde{k}_z)\mathbf{1} + \frac{2}{3}\hbar v_{\rm H}(i\sigma_3(k_x - k_y) - \sigma_2(k_x + k_y))
\end{aligned}$$

with the velocities of $v_{\rm G} = 3t_{\rm G}a_0/(2\hbar)$ and $v_{\rm H} = 3t_{\rm H}a_0/(2\hbar)$ for Graphene and Hopf-links, Dirac constant of $\hbar$, $\tilde{k}_z = k_z - 2/3$, the identity matrix $\mathbf{1}$, and Pauli matrices of σ_1, σ_2, and σ_3. The constant energy of $-t_{\rm H}$ barely shifts the bands by forming bonding and anti-bonding states between horizontal and vertical Graphene sheets by Hopf-links, and will not change the linearity. The reset of the Hamiltonian can be diagonalised and we obtained the effective Hamiltonian at $(0, 0, 2/3)$ as

$$\hat{H}_{\rm eff} = \hbar \sum_{\mathbf{k}\sigma} \hat{\Psi}^{\dagger}_{\mathbf{k}\sigma}\left(v_x k_x \sigma_1 + v_y k_y \sigma_2 + v_z k_z \sigma_3\right)\hat{\Psi}_{\mathbf{k}\sigma}, \tag{2}$$

where $\hat{\Psi}^{\dagger}_{\mathbf{k}\sigma} = \left(\alpha^{\dagger}_{\mathbf{k}\sigma}, \gamma^{\dagger}_{\mathbf{k}\sigma}\right)$ and $\hat{\Psi}_{\mathbf{k}\sigma}$ are creation and annihilation operators of quasi-particles for the valley and the velocity along z was renormalised to $v_z = (3t_{\rm G}/2 + t_{\rm H})a_0/\hbar$, while $v_x = v_y = v_{\rm G}$. Therefore, the $3D$ gapless Fermions will be obtained by the mixing of $2D$ Dirac Fermions at the degenerate Dirac point. We also obtained the flat-band, which penetrates the gapless point.

For a Hopf-link of $t_{\rm H} = 1.5$ eV, we needed to $\hat{H}$ numerically (Figs. 12-15 and Supplementary Video 5). Below, we show the dimensional crossover of gapless points realised by complex hybridisations between original linear dispersions and flat bands. We assumed that we can control $E_{\rm F}$ by doping metal such as intercalation of alkali-metal into the available slots.

3D Gapless Fermions

$3D$ gapless Fermions are characterised by massless linear dispersions along k_x, k_y, and k_z (Figs. 130 (a)-(c)). These were located near the degenerate gapless points with the energy of $E_{\rm D} = -1.0$ eV (Fig. 13). Near $E_{\rm D}$, the $3D$ Fermi surfaces should be spheroids, as found at $E_{\rm F}$ of -1.2 eV (Fig. 13 (d)) for lower valleys, and they disappeared at $E_{\rm D}$ as we increased $E_{\rm F}$. They appeared again by further increasing $E_{\rm F}$ up to -0.8 eV (Fig. 13 (e)) at the same locations in $\mathbf{k}$-space for higher valleys. We checked the linearity of the band diagram at the gapless point by plotting in both k_x-k_y (Figs. 13 (f) and 13 (g)) and k_x-k_z (Fig. 13 (b)) planes, such that the linear bands were formed between $E_3(\mathbf{k})$ and $E_1(\mathbf{k})$. It was also found that the flat-band $E_2(\mathbf{k})$ is penetrating between $E_3(\mathbf{k})$ and $E_1(\mathbf{k})$, along k_x and k_y directions, while $E_2(\mathbf{k})$ is degenerate with $E_3(\mathbf{k})$ along k_z (Fig. 13 (c)). These features are consistent with the above analytic calculations at the weak Hopf-link limit.

The gapless points found at $\mathbf{k} = (0, 0, \pm 0.74)$ accommodate triple point Fermions, recently proposed and discovered by many authors[32–35]. In the present case, the 3-fold degeneracy at each gapless point is originally coming from the sub-lattice degree of freedom and the state is described by a pseudo-spin of a Special Unitary group of degree 3, $SU(3)$. We have not included the spin-orbit interaction in the present work, because the relativistic interaction is weak in carbon based materials due to its light atomic mass of carbon. Therefore, we also have a degeneracy of spin, so that we have total 6-fold degeneracy at each gapless point. For the moment, we will not consider the spin degeneracy. This $SU(3)$ symmetry is broken away from the gapless point, since the band dispersions are combinations of linear and flat dispersions. The effective Hamiltonian is approximately given by

$$\hat{H}_{\rm eff} = \sum_{\mathbf{k}\sigma} \hat{\Psi}^{\dagger}_{\mathbf{k}\sigma} \begin{pmatrix} E_4(\mathbf{k}) & 0 & 0 & 0 \\ 0 & E_{\rm D} + \hbar v_z \tilde{k}_z & \hbar(v_x k_x - i v_y k_y) & 0 \\ 0 & \hbar(v_x k_x + i v_y k_y) & E_{\rm D} - \hbar v_z \tilde{k}_z & 0 \\ 0 & 0 & 0 & E_{\rm D} \pm \hbar \tilde{k}_z \end{pmatrix} \hat{\Psi}_{\mathbf{k}\sigma}, \tag{3}$$

where $\tilde{k}_z = k_z \pm 0.74$, $\hat{\Psi}^{\dagger}_{\mathbf{k}\sigma} = \left(\alpha^{\dagger}_{\mathbf{k}\sigma}, \beta^{\dagger}_{\mathbf{k}\sigma}, \gamma^{\dagger}_{\mathbf{k}\sigma}, \delta^{\dagger}_{\mathbf{k}\sigma}\right)$, and $\hat{\Psi}_{\mathbf{k}\sigma}$ are creation and annihilation operators after diagonalisation. Therefore, the $SU(3)$ symmetry is reduced down to $SU(2) \otimes U(1)$, so that the states are described by the 2-fold degenerate $3D$ Dirac Fermions and the 1-fold Fermions with flat-bands along k_x and k_y, while the bands are linear along k_z. The $3D$ Dirac Fermions[29,30] are essentially described by the matrix

$$\mathscr{H}_{\rm 3D} = E_{\rm D} + \hbar v \boldsymbol{\sigma} \cdot \tilde{\mathbf{k}}, \tag{4}$$

where $v \approx v_z \approx v_x = v_y$, $\boldsymbol{\sigma} = (\sigma_x, \sigma_y, \sigma_z)$, and $\tilde{\mathbf{k}} = (k_x, k_y, \tilde{k}_z)$.

2D Gapless Fermions

At the higher $E_{\rm D} = 3.2$ eV, we found $2D$ gapless Fermions at $\mathbf{k} = (0, 0, 0.48)$ (Fig. 14). Near $E_{\rm D}$, the band structures were linear along k_x (Fig. 21 (a)) and k_y (Fig. 14 (b)) , and it was almost flat along k_z (Fig. 14 (c)). Therefore, the confinement along k_z was weak, and the Fermi surface extended significantly along k_z (Figs. 14 (d) and (e)), and the Fermi surface along the k_x-k_y plane were circular, showing $2D$ characters. These $2D$ gapless Fermions are similar to those in a Graphene mono-layer. But, strictly, in Hopfene, there exists a weak dispersion along k_z as well, such that they should be described as *quasi*-$2D$, similar to strongly correlated materials such as copper-oxide superconductors[60], in contrast to the mono-layer of Graphene, where complete $2D$ confinement is achieved.

These gapless points also accommodate triple point Fermions and has the $SU(3)$ symmetry at $E_{\rm D}$. The effective Hamiltonian is approximately given by

$$\hat{H}_{\rm eff} = \sum_{\mathbf{k}\sigma} \hat{\Psi}^{\dagger}_{\mathbf{k}\sigma} \begin{pmatrix} E_{\rm D} \pm \hbar v_z \tilde{k}_z & \hbar(v_x k_x - i v_y k_y) & 0 & 0 \\ \hbar(v_x k_x + i v_y k_y) & E_{\rm D} \pm \hbar v_z \tilde{k}_z & 0 & 0 \\ 0 & 0 & E_{\rm D} & 0 \\ 0 & 0 & 0 & E_1(\mathbf{k}) \end{pmatrix} \hat{\Psi}_{\mathbf{k}\sigma}, \tag{5}$$

where $\tilde{k}_z = k_z \pm 0.48$. Therefore, 3-fold degeneracy reduces to 2-fold degeneracy and 1-fold completely flat-band along all directions. The 2-fold degenerate bands are described by $2D$ Dirac Fermions, whose effective Hamiltonian is

$$\mathscr{H}_{\rm 2D} = E_{\rm D} + \hbar v \left(\sigma_x k_x + \sigma_y k_y\right) \pm \hbar v \tilde{k}_z. \tag{6}$$

The extra linear dispersion along k_z makes the $2D$ confinement weaker.

1D Gapless Fermions

We also found *quasi*-1D gapless Fermions, due to a flat-band along the k_x-k_y plane (Figs. 15 (a) and (b)) with a massless dispersion along k_z (Fig. 15 (c)). At $E_{\rm D} = E_{\rm F} = 2.8$ eV, the highest energy states will be Fermi points along k_z (Figs. 15 (d) and (e)) The electronic properties of these states will be *quasi*-1D. We have 8 different 1D gapless points in the Brillouin zone (Figs. 15 (d) and (e)). Generations of these points would be linked to the original gapless points and flat-bands. The gapless points of Graphene and Hopf links would survive upon the introduction of the adiabatic turn-on of $t_{\rm H}$. Suppose we extend this linear dispersion from Dirac points to intersect with a flat-band, another gapless points will be generated at the crossing points. Generations should accompany both positive and negative topological charges with opposite chiralities[31], and thus the number of generated gapless points would be even. In our Hopfene, we found huge amounts of gapless points, characterised with different dimensionality.

These gapless points are composed of 2-bands, such that there is $SU(2)$ symmetry at $E_{\rm D}$ and $\mathbf{k}_{\rm D} = (1, 0, \pm 0.5)$ or $\mathbf{k}_{\rm D} = (0, 1, \pm 0.5)$. The effective Hamiltonian is approximately given by

$$\hat{H}_{\rm eff} = \sum_{\mathbf{k}\sigma} \hat{\Psi}^{\dagger}_{\mathbf{k}\sigma} \begin{pmatrix} E_{\rm D} \pm \hbar v_z \tilde{k}_z & 0 & 0 & 0 \\ 0 & E_{\rm D} \pm \hbar v_z \tilde{k}_z & 0 & 0 \\ 0 & 0 & E_2(\mathbf{k}) & 0 \\ 0 & 0 & 0 & E_1(\mathbf{k}) \end{pmatrix} \hat{\Psi}_{\mathbf{k}\sigma}, \tag{7}$$

where $\tilde{k}_z = k_z \pm 0.5$. In this case, the confinement is strong only along k_z, which is parallel to both AB and CD Graphene sheets, so that the system is close to the quasi-1D system, described by the effective Hamiltonian.

$$\mathscr{H}_{\rm 1D} = E_{\rm D} \pm \hbar v \sigma_z \tilde{k}_z. \tag{8}$$

The quasi-1D system is well-known to exhibit Tomonaga-Luttinger liquid behaviours, characterised by collective modes with spin-charge separation, when the Coulomb interaction is introduced[61].

Impact of Coulomb Interaction

Electrical properties of Hopfene are expected to be metallic, due to the lack of the band-gap in the entire spectrum (Figs. 7 and 12). The gapless dispersions of electrons are coming from the original Graphene sheets, and the 3D nested Graphene sheets ensure the electrical conduction along the entire directions. Therefore, excellent metallic properties as good as Graphene as a bulk material are expected for Hopfene. Here, we briefly discuss the impact of the Coulomb interaction on electrical properties of Hopfene.

In order to evaluate impact of the many-body Coulomb interaction, we should solve the Hubbard Hamiltonian[59,61]

$$\hat{H} = -\sum_{ij\sigma} t_{ij} \hat{\psi}^{\dagger}_{i\sigma} \hat{\psi}_{j\sigma} - E_{\rm F} \sum_{i\sigma} \hat{n}_{i\sigma} + U \sum_{i} \hat{n}_{i\uparrow} \hat{n}_{i\downarrow}, \tag{9}$$

where $\hat{\psi}^{\dagger}_{i\sigma}$ and $\hat{\psi}_{i\sigma}$ are creation and annihilation operators at the atomic lattice site i for spin σ, respectively, $\hat{n}_{i\sigma}$ is the number operator, and U is the Coulomb interaction strength. The calculated density-of-states, $D(E_{\rm F})$ is shown in Fig. 7. It is beyond the scope of this paper, to solve the 3D Hubbard model in Hopfene, but we can envisage the impact of U.

According to the Stoner's criterion[59], the flat-band ferromagnetism is expected, if $D(E_{\rm F})U > 1$, which corresponds to $U \gtrsim 10$ eV for non-doped (2,2)-Hopfene (Fig. 7). If this is satisfied, the spin degeneracy will be lifted such that the degenerate Dirac Fermions will become Weyl Fermions[62,63]. In reality, larger U will be required, since the Stoner's criterion is based on a mean-field theory and the actual requirement for ferromagnetism is more stringent in general[59].

Alternatively, if the net effective Coulomb interaction becomes attractive, superconductivity is expected[64,59]. The flat-band condition is also favourable for superconductivity. There are many carbon based allotropes, which shows superconductivity such as intercalated graphites[65,66], K_3C_{60}[54], carbon-nano-tube[67,68], Q-Carbon[69], and twisted bilayer Graphene[70]. Theoretically, the arbitrary weak attractive interaction, $U < 0$, is enough to allow the instability towards superconductivity[64,59], so that the strong interaction is not required. The transition temperature depends on $D(E_{\rm F})$ and U, and it is expected to have a crossover[71] from the weak coupling BCS limit to the strong coupling Bose-Einstein Condensation (BEC) by increasing $|U|$[53].

Conclusion

We have considered the concept of topological materials[8–10] in materials with hard covalent bonds. 1D Carbon-Nano-Chains, Hopf-linked bilayer-Graphene (2D), and 3D Hopfene have been proposed as examples of new *topological carbon allotropes*, which will be useful to examine fundamental physics of massless Dirac Fermions[4,23,31,45,55] in topologically nontrivial

geometries. We envisage various practical applications (Supplementary Fig. 7) of these hard and flexible topological materials for DNA-sensing, functional materials, and NEMS.

It is straightforward to extend this concept[8–10] to make *heterogeneous topological structures* by introducing different materials such as boron-nitride and molybdenum-disulfide. The unique aspect of this approach is a topological link to bind various sheets strongly together without forming a proper chemical bond. This configuration is *topologically different* from the simple stacking weakly bound together by van der Waals force[72].

As the first step towards making Hopfene, we propose to make Hopf-linked bilayer-Graphene (Fig. 8). Unlike to the stacked bilayer-Graphene[4–7], the Graphene sheets are linked only at the $1D$ chain, so that the impacts of the coupling on the band structure would be limited. Reflecting the double layers, momentum space will also be double, leading to the crossed layers even in momentum space (Fig. 8b). The valleys are degenerate at the same points, because the direction of the zig-zag edge (z) is the same for both layers due to sharing of the $1D$ chain. As we increase the number of inserted Graphene sheets, momentum space will be eventually filled by layers towards the complete $3D$ band structure. It is beyond the scope of this paper to predict how the $2D$ Dirac Fermions[4,23,31,45,55] are crossing over to $3D$ Dirac Fermions in Hopfene.

In conclusion, the electronic structures of the $3D$ Hopf-linked honeycomb lattices, named Hopfene, show the distinctive topological features characterised by $3D$, $2D$, and $1D$ gapless Fermions. The Fermi surfaces show dimensional crossover upon changes of the Fermi level. The impact of topological structures on electrical properties is significant and these materials will be useful as platforms to examine various concepts of physics including magnetic monopoles, geometrical phases, and topological superconductors. One can explore even more interesting topologically non-trivial crystal structures.

References

1. Nambu, Y. Quasi-particles and gauge invariance in the theory of superconductivity. *Phys. Rev.* **117**, DOI: 10.1103/PhysRev.117.648 (1960).
2. Kroto, H. W., Heath, J. R., O'Brien, S. C., Curl, R. F. & Smalley, R. E. C_{60}: Backminsterfullerene. *Nature* **318**, 162–163, DOI: 10.1038/318162a0 (1985).
3. Iijima, S. Helical microtubules of graphitic carbon. *Nature* **354**, 56–58, DOI: 10.1038/354056a0 (1991).
4. Ando, T. Theory of electronic states and transport in carbon nanotubes. *J. Phys. Soc. Jpn.* **74**, 777–817, DOI: 10.1143/JPSJ.74.777 (2005).
5. Oshima, C. & Nagashima, A. Ultra-thin epitaxial films of graphite and hexagonal boron nitride on solid surfaces. *J. Phys.: Condens. Metter* **9**, 1–20, DOI: 10.1088/0953-8984/9/1/004 (1997).
6. Novoselov, K. S. *et al.* Electric field effect in atomically thin carbon films. *Science* **306**, 666–669, DOI: 10.1126/science.1102896 (2004).
7. Ferrari, A. C. *et al.* Raman spectrum of graphene and graphene layers. *Phys. Rev. Lett.* **97**, 187401, DOI: 10.1103/PhysRevLett.97.187401 (2006).
8. MacGillivray, L. R., Subramanian, S. & Zaworotko, M. J. Interwoven two- and three-dimensional coordination polymers through self-assembly of Cu' cations with linear bidentate ligands. *J. Chem. Soc., Chem. Commun.* **0**, 1325–1326, DOI: 10.1039/C39940001325 (1994).
9. Carlucci, L., Ciani, G. & Proserpio, D. M. Polycatenation, polythreading and polyknotting in coordination network chemistry. *Coord. Chem Rev.* 247–289, DOI: 10.1016/S0010-8545(03)00126-7 (2003).
10. Proserpio, D. M. Polycatenation weaves a 3d web. *Nat. Chem.* **2**, 435–436, DOI: 10.1038/nchem.674 (2010).
11. Bissell, R. A., Córdova, E., Kaifer, A. E. & Stoddart, J. F. A chemically and electrochemically switchable molecular shuttle. *Nature* **369**, 133–137, DOI: 10.1038/369133a0 (1994).
12. Fang, L. *et al.* Mechanically bonded macromolecules. *Chem. Soc. Rev.* **39**, 17–29, DOI: 10.1039/b917901a (2010).
13. v. d. Molen, S. J. *et al.* Light-controlled conductance switching of ordered metal-molecule-metal devices. *Nano Lett.* **9**, 76–80, DOI: 10.1021/nl802487j (2009).
14. Sauvage, J. P. From chemical topology to molecular machines (Nobel lecture). *Angew. Chem. Int. Ed.* **56**, 11080–11093, DOI: 10.1002/anie.201702992 (2017).
15. Dabrowski-Tumanski, P. & Sulkowska, J. I. Topological knots and links in proteins. *PNAS* **114**, 3415–3420, DOI: 10.1073/pnas.1615862114 (2017).
16. Hopf, H. Über die abbildungen der dreidimensionalen sphäre auf die kugelfläche. *Math. Annalen* **104**, 637–665, DOI: 10.1007/BF01457962 (1931).

17. Sunada, T. Lecture on topological crystallography. *Jpn. J. Math.* **7**, 1–39, DOI: 10.1007/s11537-012-1144-4 (2012).

18. Thurston, W. P. Three dimentional manifolds, Kleinian groups and hyperbolic geometry. *Bull. Amer. Math. Soc. (N.S.)* **6**, 357–381, DOI: projecteuclid.org/euclid.bams/1183548782 (1982).

19. Perelman, G. Finite extinction time for the solutions to the ricci flow on certain three-manifolds. *arXiv:math/0307245 [math.DG]* (2003).

20. Berezinskii, V. L. Destruction of long-range order in one-dimensional and two-dimensional systems having a continuous symmetry group i. classical systems. *Sov. Phys. JETP* **32**, 493–500 (1971).

21. Kosterlitz, J. M. & Thouless, D. J. Long range order and metastability in two dimensional solids and superfluids. *J. Phys. C: Solid State Phys.* **5**, L124–L126 (1972).

22. Tanda, S. *et al.* A möbius strip of single crystals. *Nature* **417**, 397–398, DOI: 10.1038/417397a (2002).

23. Kane, C. L. & Mele, E. J. z_2 topological order and the quantum spin hall effect. *Phys. Rev. Lett.* **95**, 146802, DOI: 10.1103/PhysRevLett.95.146802 (2005).

24. Hsieh, D. *et al.* A topological Dirac insulator in a quantum spin Hall phase. *Nature* **452**, 970–974, DOI: 10.1038/nature06843 (2008).

25. Ovchinnikov, A. A. & i. L. Shamovsky. The structure of the ferromagnetic phase of carbon. *J. Mol. Struct. THEOCHEM* **251**, DOI: 10.1016/0166-1280(91)85138-W (1991).

26. Kittel, C. *Introduction to Solid State Physics* (John Wiley & Sons, 2004), 8 edn.

27. Wallace, P. R. The band theory of graphite. *Phys. Rev* **71**, 622–634 (1946).

28. CastroNeto, A. H., Guinea, F., Peres, N. M. R., Novoselov, K. S. & Geim, A. K. The electronic properties of graphene. *Rev. Mod. Phys.* **81**, 109–162, DOI: 10.1103/RevModPhys.81.109 (2009).

29. Wang, Z. *et al.* Dirac semimetal and topological phase transitions in A_3Bi (A=Na, K, Rb. *Phys. Rev. B* **85**, 195320, DOI: 10.1103/PhysRevB.85.195320 (2012).

30. Liu, Z. K. *et al.* Discovery of a three-dimensional topological Dirac semimetal, Na_3Bi. *Science* **343**, 864–867, DOI: 10.1126/science.1245085 (2014).

31. Armitage, N. P., Mele, E. J. & Vishwanath, A. Weyl and Dirac semimetals in three-dimensional solids. *Rev. Mod. Phys.* **90**, DOI: 10.1103/RevModPhys.90.015001 (2018).

32. Zhu, L. *et al.* Blue phosphorene oxide: Strain-tunable quantum phase transitions and novel 2d emergent fermions. *Nano Lett.* **16**, 6548–6554, DOI: 10.1021/acs.nanolett.6b03208 (2016).

33. Bradlyn, B. *et al.* Beyond Dirac and Weyl fermions: Unconventional quasiparticles in conventional crystals. *Science* **353**, aaf5037, DOI: 10.1126/science.aaf5037 (2016).

34. Chang, G. *et al.* Nexus fermions in topological symmorphic crystalline metals. *Sci. Rep.* **7**, 1688, DOI: 10.1038/s41598-017-01523-8 (2016).

35. Lv, B. Q. *et al.* Observation of threee-component fermions in the topological semimetal molybdenum phosphide. *Nature* **546**, 627–631, DOI: 10.1038/nature22390 (2017).

36. Mermin, N. D. & Wagner, H. Absence of ferromagnetism or antiferromagnetism in one- or two-dimensional isotropic Heisenberg models. *Phys. Rev. Lett.* **17**, 1133–1136, DOI: https://doi.org/10.1103/PhysRevLett.17.1133 (1966).

37. Hohenberg, P. C. Existence of long-range order in one and two dimensions. *Phys. Rev.* **158**, 383–386, DOI: 10.1103/PhysRev.158.383 (1967).

38. Metzner, W. & Vollhardt, D. Correlated lattice fermions in $d = \infty$ dimensions. *Phys. Rev. Lett.* **62**, 324–327, DOI: 10.1103/PhysRevLett.62.324 (1989).

39. Georges, A., Kotliar, G., Krauth, W. & Rozenberg, M. J. Dynamical mean-field theory of strongly correlated fermion systems and the limit of infinite dimensions. *Rev. Mod. Phys.* **68**, 13–125, DOI: 10.1103/RevModPhys.68.13 (1996).

40. Evans, D. A. History of the Harvard ChemDraw project. *Angew. Chem. Int. Ed.* **53**, 11140–11145, DOI: 10.1002/anie.201405820 (2014).

41. Van, N. H., Muruganathan, M., Kulothungan, J. & Mizuta, H. Fabrication of a three-terminal graphene nanoelectromechanical switch using two-dimensional materials. *Nanoscale* **10**, 12349, DOI: 10.1039/c7nr08439k (2018).

42. Kim, K. S. *et al.* Large-scale pattern growth of graphene films for stretchable transparent electrodes. *Nature* **457**, 706–710, DOI: 10.1038/nature07719 (2009).

43. Segawa, Y. *et al.* Topological molecular nanocarbons: All-benzene catenane and trefoil knot. *Science* **365**, 272–276, DOI: 10.1126/science.aav5021 (2019).

44. Kaiser, K. *et al.* An sp-hybridized molecular carbon allotrope, cyclo[18]carbon. *Science* **365**, 1299–1301, DOI: 10.1126/science.aay1914 (2019).

45. Nakada, K., Fujita, M., Dresselhaus, G. & Dresselhaus, M. S. Edge state in graphene ribbons: Nanometer size effect and edge shape dependence. *Phys. Rev. B* **54**, 17954–17961 (1996).

46. Flouris, K., Jimenez, M. M. & Herrmann, H. J. Quantum spin-Hall effect on Möbius graphene ribbon. *arXiv:1902.03892 [cond-mat.mes-hall] arXiv:1902.03892 [cond-mat.mes-hall]* (2019).

47. Herges, R. Topology in chemistry: Designing möbius molecules. *Chem. Rev.* **106**, 4820–4842, DOI: 10.1021/cr0505425 (2006).

48. Chichak, K. S. *et al.* Molecular borromean rings. *Science* **304**, 1308–1312, DOI: 10.1126/science.1096914 (2004).

49. Peters, A. J., Chichak, K. S., Cantrill, S. J. & Stoddart, J. F. Nanoscale borromean links for real. *Chem. Comm.* **27**, 3394–3396, DOI: 10.1039/b505730b (2005).

50. Shirakawa, H., Louis, E. J., Macdirmid, A. G., Chiang, C. K. & Heeger, A. J. Synthesis of electrically conducting organic polymers: Halogen derivatives of polyacetylene, $(CH)_x$. *J. C. S. Chem. Comm.* 578–580, DOI: 10.1039/C39770000578 (1977).

51. Shapere, A. & Wilczek, F. Classical time crystals. *Phys. Rev. Lett.* **109**, DOI: 10.1103/PhysRevLett.109.160402 (2012).

52. Tomita, I. & Saito, S. Lattice deformation on flat-band modulation in 3d Hopf-linked carbon allotrope: Hopfene. *Appl. Phys. Lett.* **115**, DOI: 10.1063/1.5118967 (2019).

53. Saito, S. & Tomita, I. BCS-BEC crossover and superconductor-insulator transition in Hopf-linked Graphene layers: Hopfene. *Mater. Res. Express* **6**, DOI: 10.1088/2053-1591/ab4337 (2019).

54. Hebard, A. F. *et al.* Superconductivity at 18 K in potassium-doped C_{60}. *Nature* **350**, 600–601, DOI: 10.1038/350600a0 (1991).

55. Sorella, S. *et al.* Correlation-driven dimerization and topological gap opening in isotropically strained graphene. *Phys. Rev. Lett.* **121**, 066402, DOI: 10.1103/PhysRevLett.121.066402 (2018).

56. Giannozzi, P. *et al.* Quantum ESPRESSO: a modular and open-source software project for quantum simulations of materials. *J. Phys: Condens. Matter* **21**, 395502, DOI: 10.1088/0953-8984/21/39/395502 (2009).

57. Hu, J. *et al.* Three-dimensional honycomb carbon: Junction line distortion and novel emergent fermions. *Carbon* **141**, 417–426, DOI: 10.1016/j.carbon.2018.09.027 (2019).

58. Wang, B. & Ohgushi, K. Post-perovskite transition in anti-structure. *Sci. Rep.* **6**, 37896, DOI: 10.1038/srep37896 (2016).

59. Auerbach, A. *Interacting Electrons and Quantum Magnetism* (Springer, 1994).

60. Bednorz, J. G. & Müller, K. A. Possible highT_c superconductivity in the Ba-La-Cu-O system. *Z. Physik B - Condens. Matter* **64**, 189–193, DOI: 10.1007/BF01303701 (1986).

61. Giamarchi, T. *Quantum Physics in One Dimension* (Oxford University Press, 2004).

62. Weng, H., Fang, C., Fang, Z., Bernevig, B. A. & Dai, S. Weyl semimetal phase in noncetrosymmetric transition-metal monophosphides. *Phy. Rev. X* **5**, 011029, DOI: 10.1103/PhysRevX.5.011029 (2015).

63. Xu, S. Y. *et al.* Discovery of a Weyl fermion semimetal and topological Fermi arcs. *Science* **349**, 613–617, DOI: 10.1126/science.aaa9297 (2015).

64. Bardeen, J., Cooper, L. N. & Schrieffer, J. R. Theory of superconductivity. *Phys. Rev.* **108**, 1175–1204 (1957).

65. Belash, I. T., Zharikov, O. V. & Palnichenko, A. V. Superconductivity of GIC with Li, Na and K. *Synth. Met.* **34**, 455–460, DOI: 10.1016/0379-6779(89)90424-4 (1989).

66. Emery, N., Hérold, C., Marêché, J. F. & Lagrange, P. Synthesis and superconducting properties of cac6. *Sci. Technol. Adv. Mater.* **9**, 044102, DOI: 10.1088/1468-6996/9/4/044102 (2008).

67. Kamide, K., Kimura, T., Nishida, M. & Kurihara, S. Singlet superconductivity phase in carbon nanotubes. *Phys. Rev. B* **68**, 024506, DOI: 10.1103/PhysRevB.68.024506 (2003).

68. Cleuziou, J. P., Wernsdorfer, W., Bouchiat, V., Ondarçuhu, T. & Monthioux, M. Carbon nanotube superconducting quantum interference device. *Nat. Nanotech.* **1**, 53–59 (2006).

69. Bbhaumik, A., Sachan, R., Gupta, S. & Narayan, J. Discovery of high-temperature superconductivity (tc=55k) in b-doped q-carbon. *ACS NANO* **22**, 11915–11922, DOI: 10.1021/acsnano.7b06888 (2017).

70. Cao, Y. *et al.* Unconventional superconductivity in magic-angle graphene superlattices. *Nature* **556**, 43–50 (2018).

71. Micnas, R., Ranninger, J. & Robaskiewicz, S. Superconductivity in narrow-band systems with local nonretarded attractive interactions. *Rev. Mod. Phys.* **62**, 113–171 (1990).

72. Koma, A., Sunouchi, K. & Miyajima, T. Fabrication of ultrathin heterostructures with van der Waals epitacy. *J Vac Sci Technol B* **3**, DOI: 10.1116/1.583125 (1985).

Acknowledgements

This work is supported by EPSRC Manufacturing Fellowship (EP/M008975/1). We would like to thank Prof. H. Mizuta, Dr. M. Muruganathan, Prof. Y. Oshima, Prof. S. Matsui, Prof. S. Ogawa, Prof. S. Kurihara, and Prof. H. N. Rutt for stimulating discussions. S.S also would like to thank JAIST for their hospitalities during his stay at the Center for Single Nanoscale Innovative Devices.

Author contributions statement

S.S. and I.T. conceived the idea of topological carbon allotropes, together. S.S. conceived the simulations, and I.T. analysed the results. S.S. wrote the draft. S.S. and I.T. reviewed the manuscript.

Additional information

Accession codes (The data from the paper can be obtained from the University of Southampton ePrint research repository: http://dx.doi.org/10.5258/SOTON/D0884); **Competing interests** (The authors declare no competing interests both financially and non-financially.).

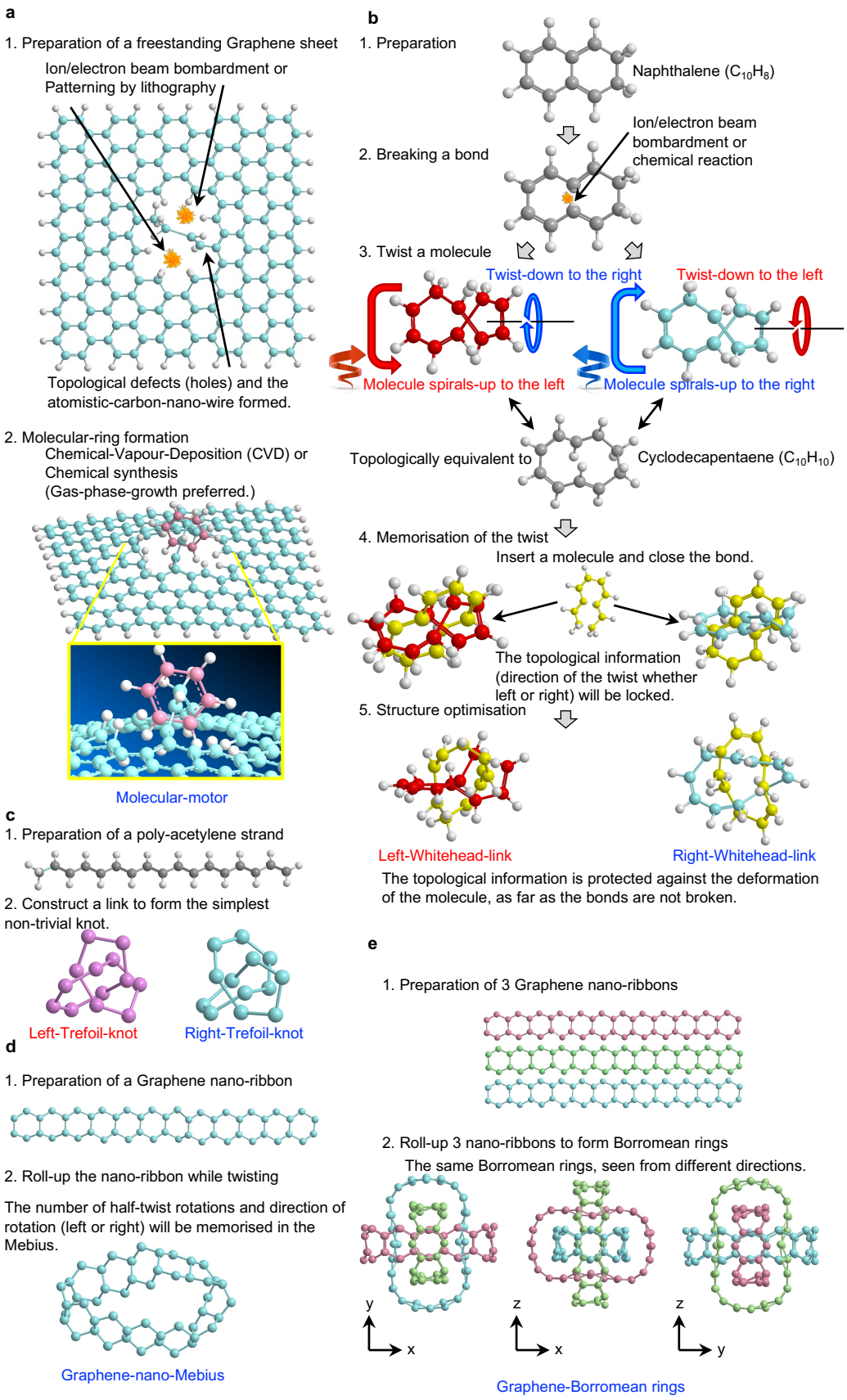

Figure 1. Proposed procedure to make topological structures. a, Benzene-based molecular motor. A Graphene sheet is prepared, and patterned to form an atomic wire using ion/electron beam or lithography. Then, a benzene or other organic molecule is trapped in the patterned atomic wire. **b**, Whitehead-links. Left and right links will be created by twisting molecules and locked by another atomic wires. **c**, Trefoil-knots. Left and right knots can be created depending on how to connect the atomic wire. **d**, Möbius strip using a Graphene nano-ribbon. **e**, Borromean rings using Graphene nano-ribbons.

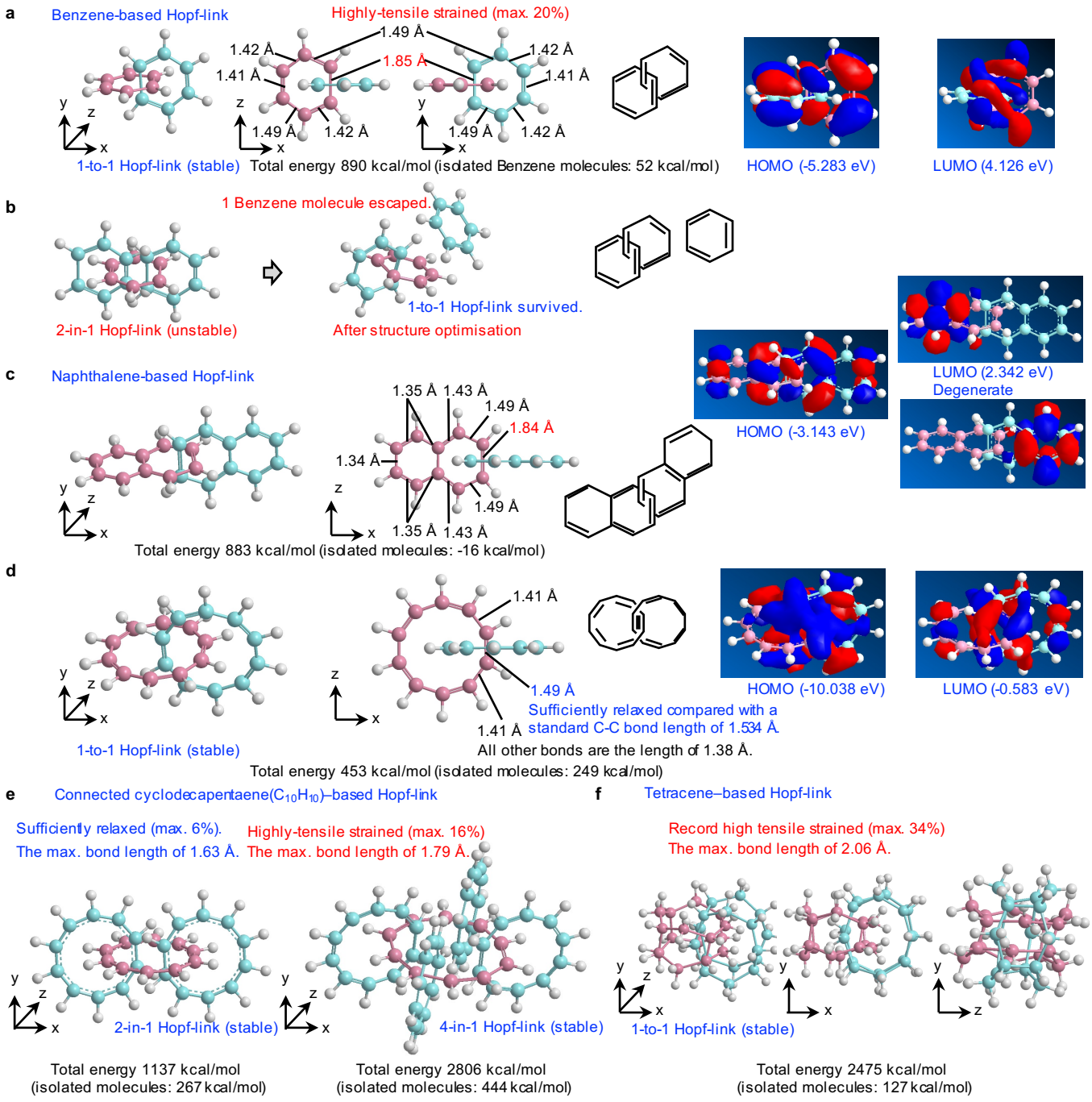

Figure 2. Hopf-linked molecules. a, Benzene-based Hopf-linked molecule. The bonds penetrating into the other benzene ring were highly-strained. The linked benzene rings are intersecting perpendicular to each other, and there are energetically-equivalent 6 positions corresponding to the sides of each ring, so that the total $6 \times 6 = 36$ configurations are allowed corresponding to its hexagonal structure. Wavefunctions for both HOMO and LUMO are spreading to the entire link, suggesting the strong hybridisation of 2 rings. **b**, Break-down of benzene-based Hopf-linked molecule. A benzene ring can accommodate only 1 benzene-ring. **c**, Naphthalen-based Hopf-linked molecule. A building block to construct a chain using a benzene ring. In this case, we expect $5 \times 5 = 25$ configurations for each Hopf-linked molecule, depending on the relative angle and the position of Naphthalene molecules. **d**, Cyclodecapentaene-based Hopf-linked molecule. The strains of bonds are significantly relaxed. **e**, Accommodations of 2 and 4 rings into cyclodecapentaene-based Hopf-linked molecule. **f**, Tetracene-based Hopf-linked molecule. Graphene nano-ribbons can also be used to construct a Hopf-links

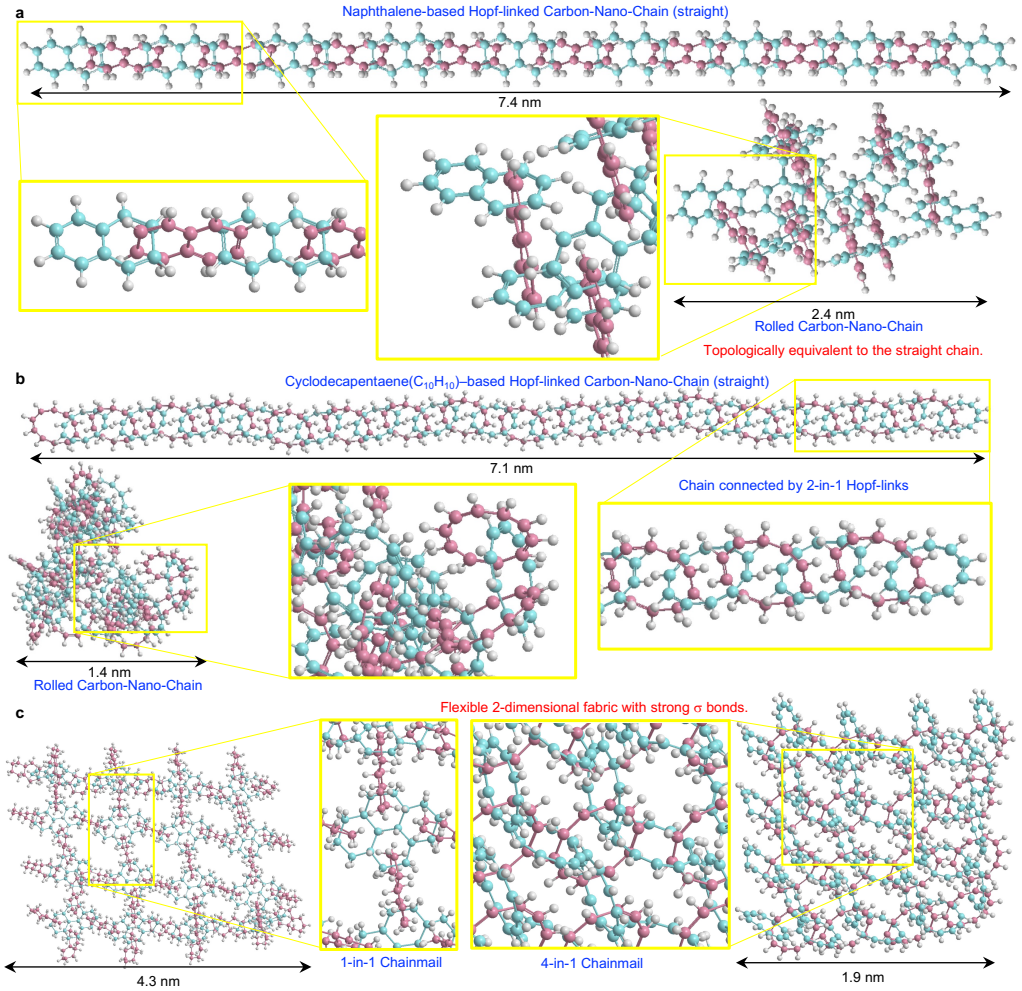

Figure 3. Carbon-Nano-Chains and Chainmail. a, Naphthalene-based Hopf-linked chain. The chain can change the global geometries without changing the topology of the chain protected by strong σ bonds. **b**, Cyclodecapentaene-based Hopf-linked chain. Straight and rolled chains are topologically the same, keeping the robust Topological-Long-Range-Order, while the translational symmetries are broken due to its flexible nature of the chain. **c**, Chainmail using Hopf-links. Only 1 benzene ring can enter into another benzene ring, while cyclodecapentaene ($C_{10}H_{10}$) can accommodate the maximum of 4 rings.

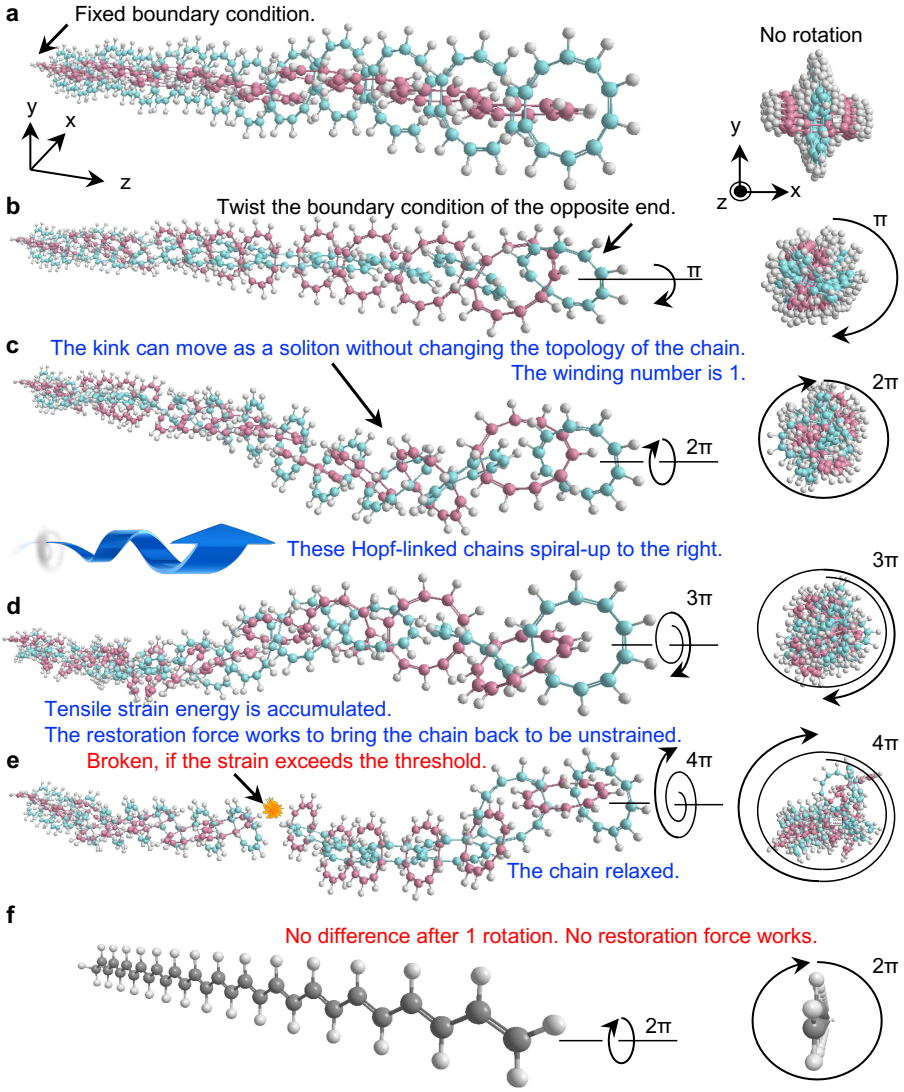

Figure 4. Stability of Hopf-linked Chain. The stability of the chain was examined by imposing a fixed boundary condition. **a**, Original straight-chain. No global strain was accumulated. **b**, π-twisted chain. One of the ring at the boundary was π rotated to the right. **c**, 2π-twisted chain. The winding number of the chain is 1, so that the kink appeared as a soliton, which is topologically protected upon deformations of the chain. **d**, 3π-twisted chain. The restoration forces worked to bring the chain back to the straight line. **e**, 4π-twisted chain. The chain was broken down and the strain was relaxed. **f**, Poly-acetylene chain. No restoration force worked upon the rotation of 2π due to its rotational symmetry.

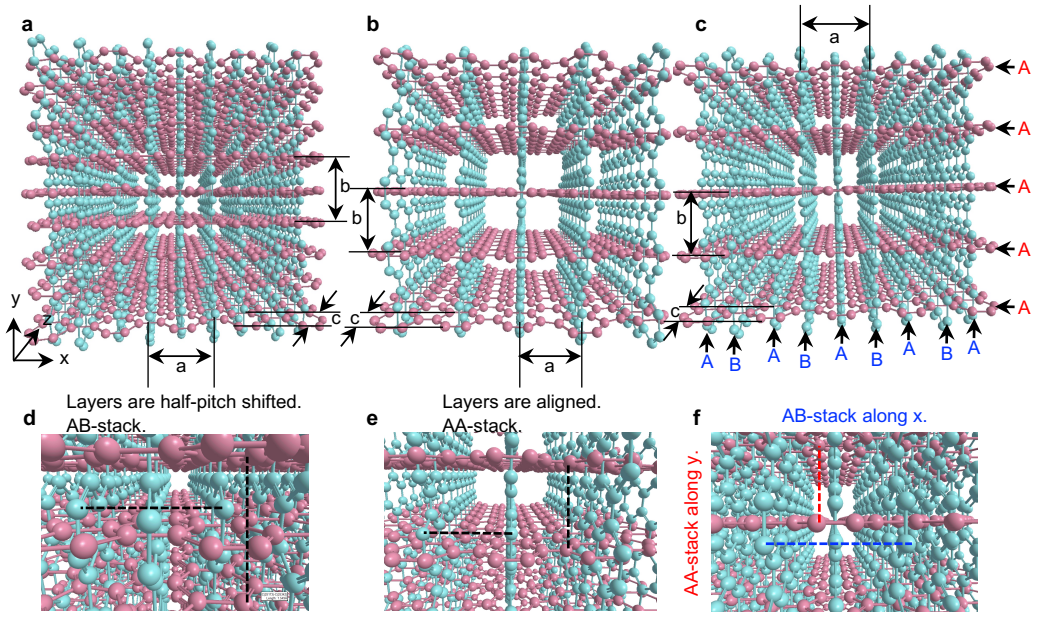

Figure 5. New 3*D* **carbon allotrope, Hopfene. a**, (1,1) Hopfene with the maximum insertions of Graphene sheets in the unit cell with AB-stacks. It is a tetrahedral structure with the lattice constant $a = b$. **b**, (2,2) Hopfene with aligned AA-stacks adjacent Graphene layers. It is also a tetrahedral structure with the lattice constant $a = b$. **c**, (1,2) Hopfene with AB stacks along horizontal (x) direction and AA-stacks along vertical direction (y) . It is also a tetrahedral structure with the lattice constant $a = b$. **d-f**, Expanded views of (1,1), (2,2), and (1,2) Hopfene crystals.

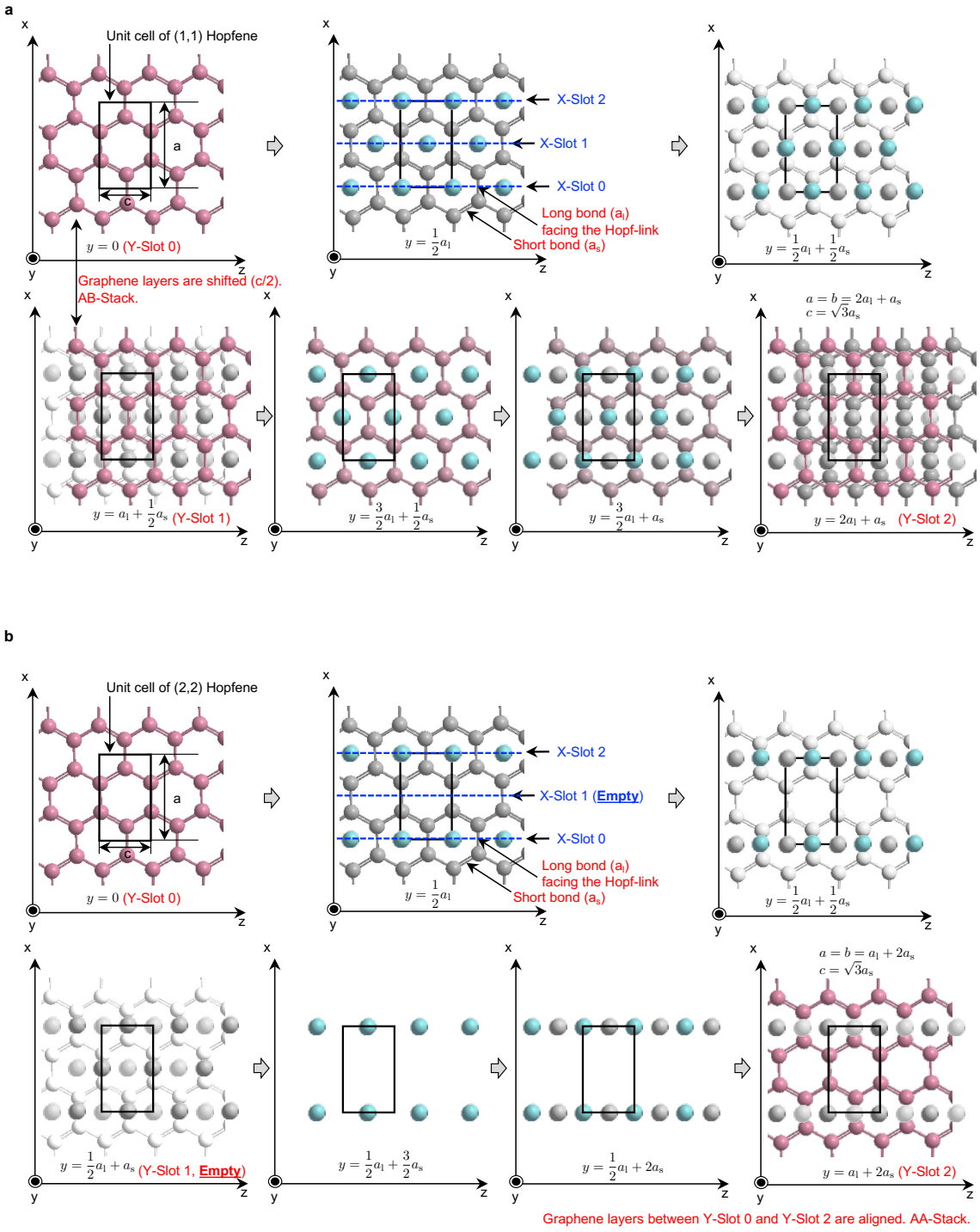

Figure 6. Unit cells for (1,1) and (2,2) Hopfene structures. The crystal structure is tetragonal for both structures ($a = b \neq c$). We show the details of atomic arrangements in unit cells upon increasing the layers. The bond length of the bond across the Hopf-link was expanded to be long a_l, while the expansion of other bonds was shorter a_s. **a**, Unit cell for (1,1) Hopfene. All available slots are occupied by Hopf-links. We obtained $a_l = 1.8$ and $a_l = 1.5$. The lattice constants were $a = b = 2a_l + a_s = 5.1$ and $c = \sqrt{3}a_s = 2.6$. **b**, Unit cell for (2,2) Hopfene. The middle slot (slot 1) in the unit cell is empty for both x and y directions. We obtained $a_l = 1.8$ and $a_l = 1.4$. The lattice constants are $a = b = a_l + 2a_s = 4.6$ and $c = \sqrt{3}a_s = 2.4$.

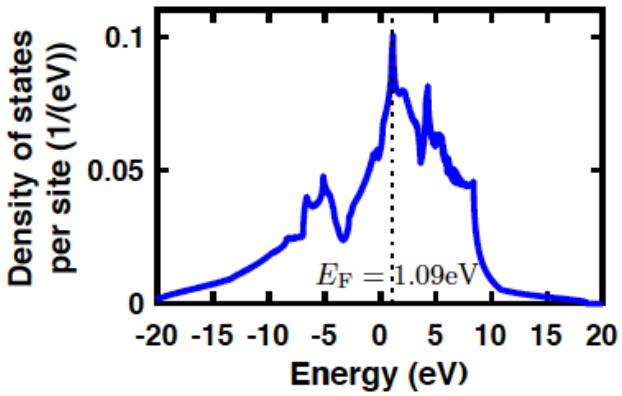

Figure 7. Density of states of (2,2)-Hopfene.

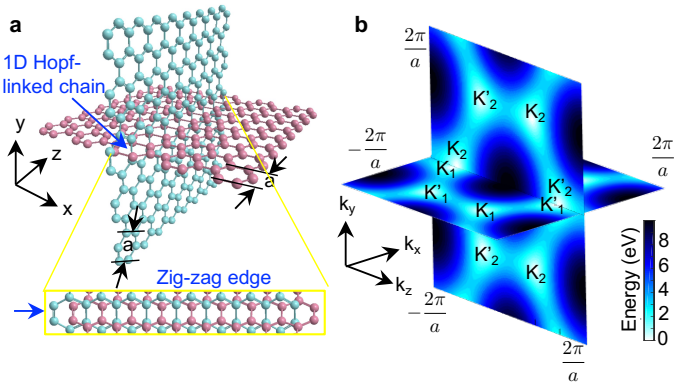

Figure 8. Hopf-linked bilayer-Graphene. a, Simulated structure. 1*D* Hopf-linked chain was made at the intersection. The bonds were expanded in the chain, while other bonds away from the link was fully relaxed due to its open boundary condition during the simulation. **b**, Expected electronic band structure, calculated by the tight-binding approximations. The horizontal Graphene has 2 valleys at K_1 and $K_1^{'}$, while the vertical one has 2 valleys at K_2 and $K_2^{'}$. K_1 ($K_1^{'}$) and K_2 ($K_2^{'}$) are located at the equivalent position in the momentum space, so that states are completely degenerate at these points, while the propagating sheets in real space are different.

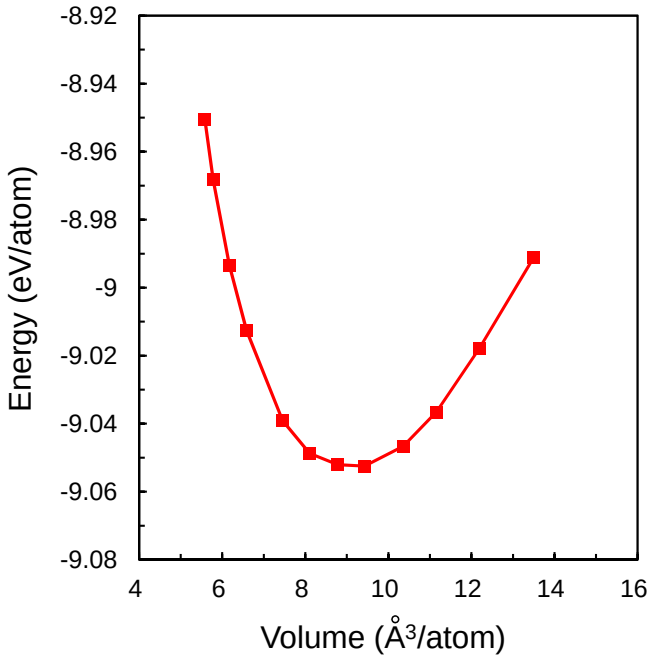

Figure 9. Stability of (2,2)-Hopfene. The energy is calculated as a function of the volume by *ab-initio* Density Functional Theory (DFT).

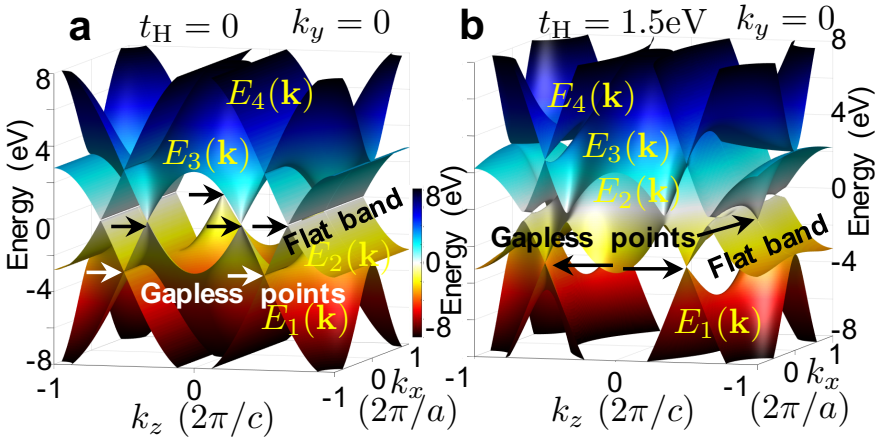

Figure 10. 3*D* band structures of (2,2)-Hopfene at $k_y=0$ with the transfer energies of the Hopf-links of (a) $t_{\rm H}=0$ and (b) $t_{\rm H}=1.5$ eV.

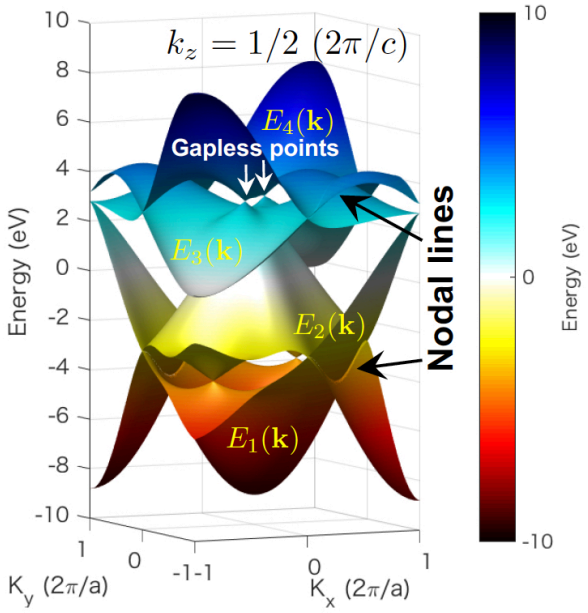

Figure 11. $3D$ band structures of (2,2)-Hopfene at $k_z = 1/2$, showing nodal lines.

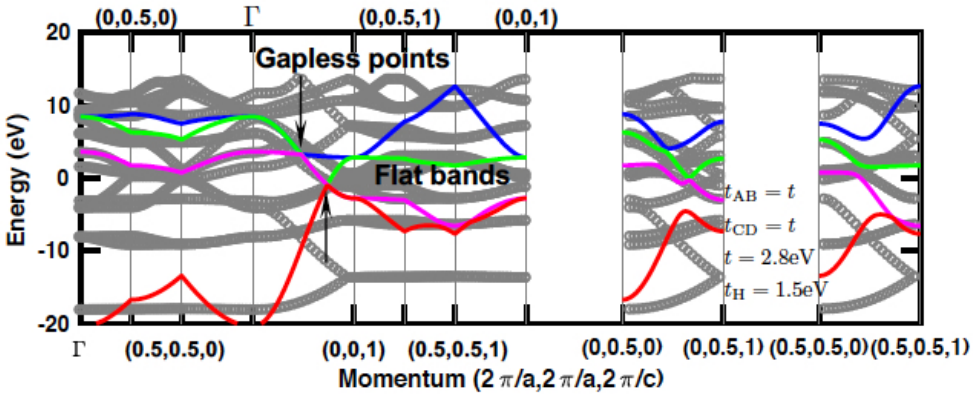

Figure 12. Band structures of (2,2)-Hopfene at $t_G = 2.8$ eV and $t_H = 1.5$ eV. The tight-binding calculations are shown by lines and the first principle calculations are shown by circles.

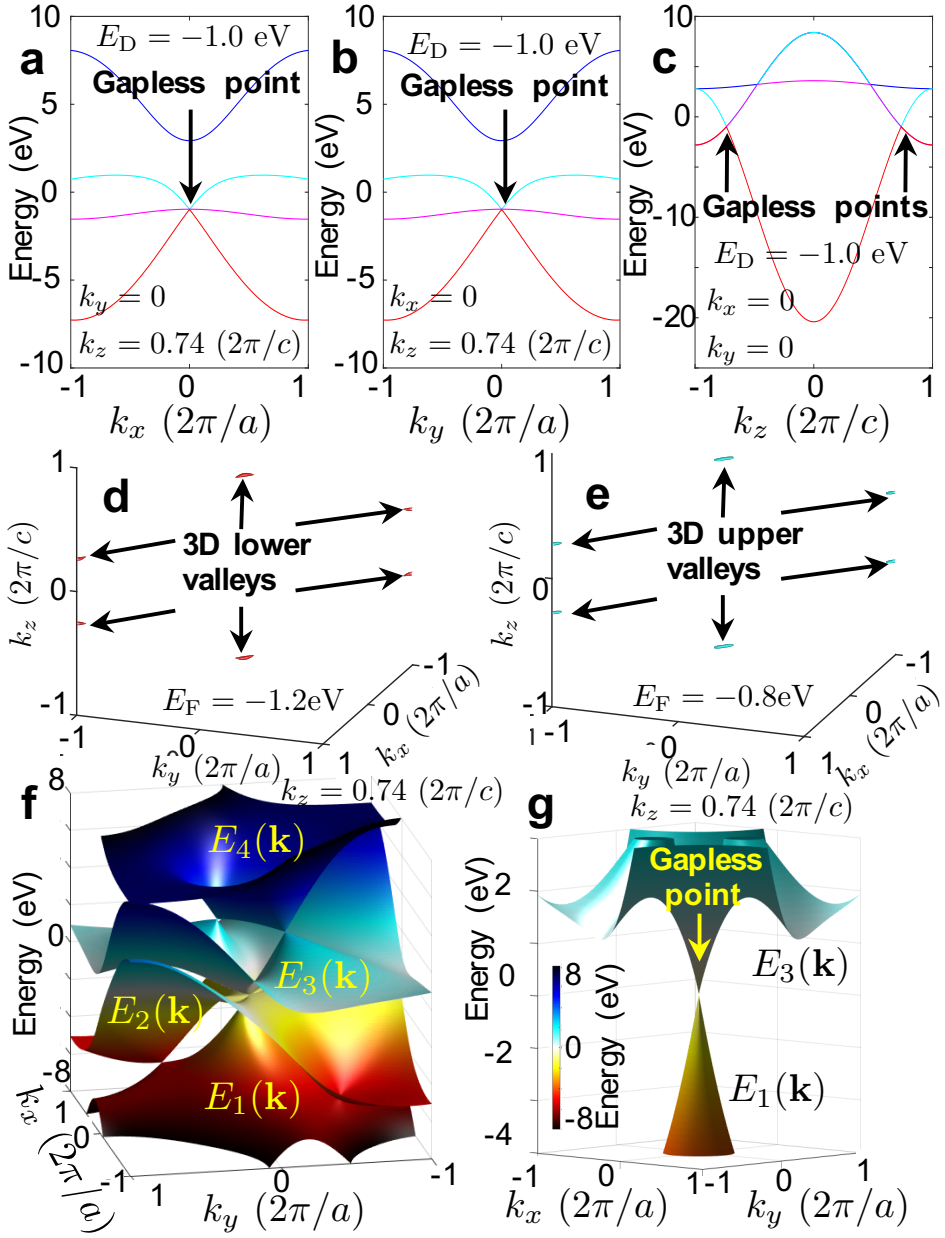

Figure 13. 3*D* gapless Fermions of (2,2)-Hopfene. Band structures at Dirac point $\mathbf{k} = (0, 0, 0.74)$ along (a) x, (b) y, and (c) z directions. Fermi surfaces of (d) lower and (e) upper valleys are also shown, proving the 3*D* feature. (f) Energy band diagram in the k_x-k_y plane at $k_z = 0.74$, showing (a) linear dispersions of $E_3(\mathbf{k})$ and $E_1(\mathbf{k})$ with the flat band $E_2(\mathbf{k})$ in-between.

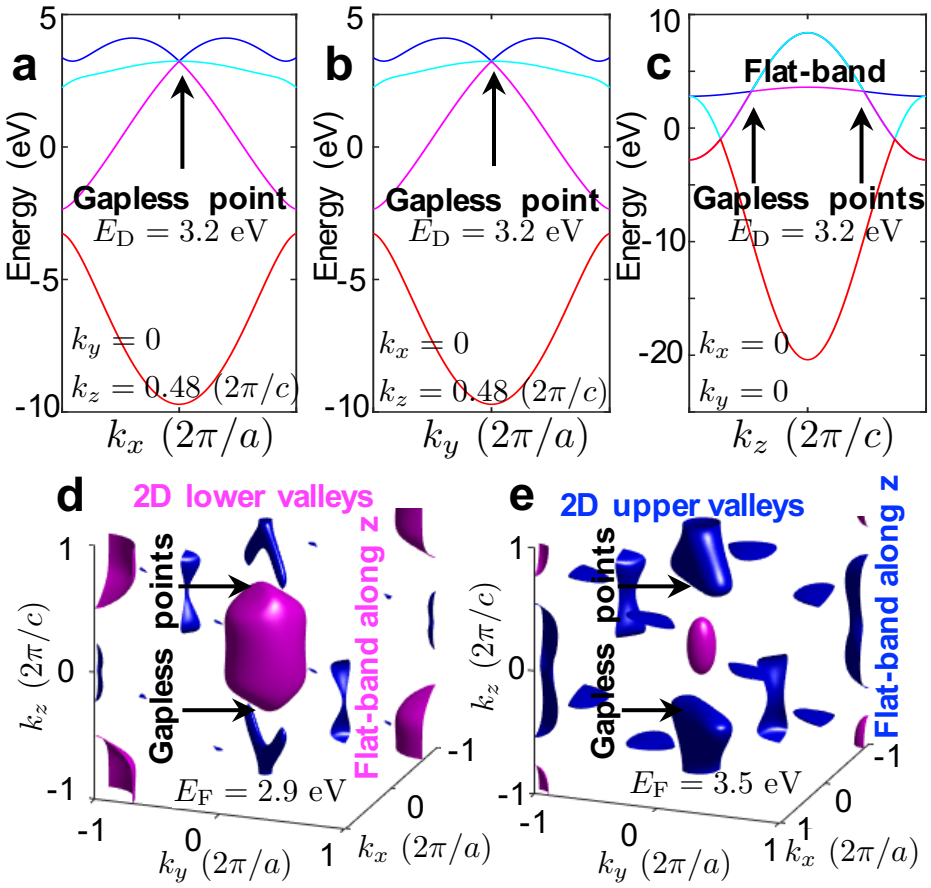

Figure 14. 2*D* gapless Fermions of (2,2)-Hopfene. Band structures at Dirac point $\mathbf{k} = (0, 0, 0.48)$ along (a) x, (b) y, and (c) z directions. Fermi surfaces of (d) lower and (e) upper valleys.

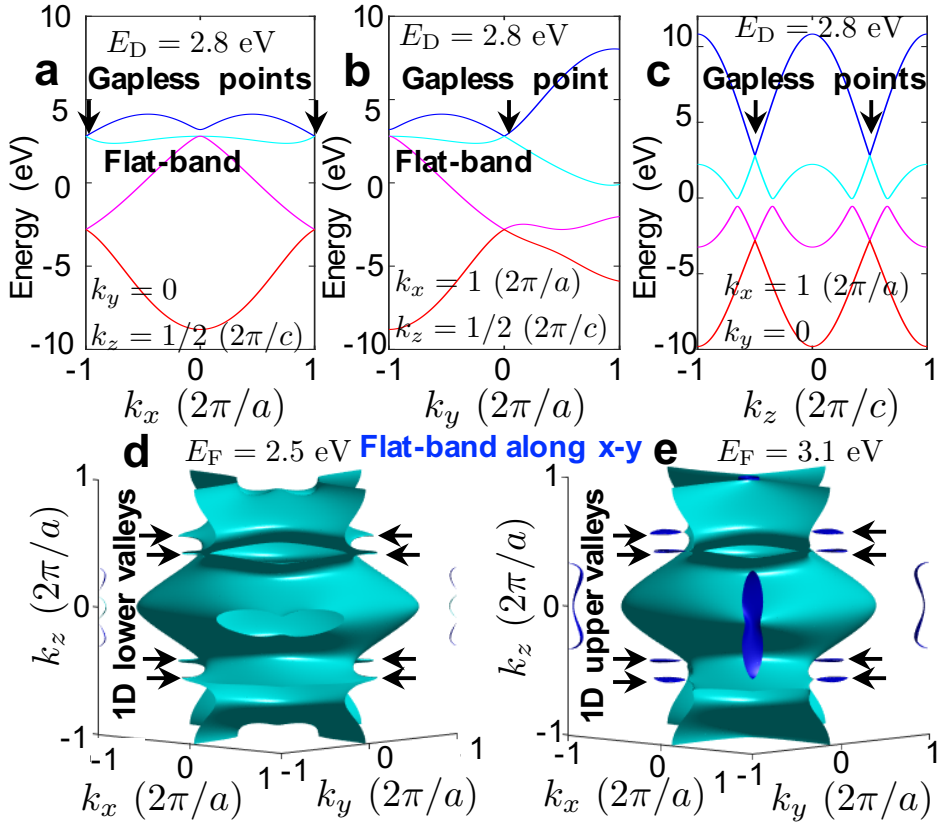

Figure 15. 1*D* gapless Fermions of (2,2)-Hopfene. Band structures at Dirac point $\mathbf{k} = (1, 0, 1/2)$ at $E_D = 2.8$ eV along (a) x, (b) y, and (c) z directions. Fermi points of (d) lower and (e) upper valleys.

References

1. Nambu, Y. Quasi-particles and gauge invariance in the theory of superconductivity. *Phys. Rev.* **117**, DOI: 10.1103/PhysRev.117.648 (1960).
2. Kroto, H. W., Heath, J. R., O'Brien, S. C., Curl, R. F. & Smalley, R. E. C_{60}: Backminsterfullerene. *Nature* **318**, 162–163, DOI: 10.1038/318162a0 (1985).
3. Iijima, S. Helical microtubules of graphitic carbon. *Nature* **354**, 56–58, DOI: 10.1038/354056a0 (1991).
4. Ando, T. Theory of electronic states and transport in carbon nanotubes. *J. Phys. Soc. Jpn.* **74**, 777–817, DOI: 10.1143/JPSJ.74.777 (2005).
5. Oshima, C. & Nagashima, A. Ultra-thin epitaxial films of graphite and hexagonal boron nitride on solid surfaces. *J. Phys.: Condens. Metter* **9**, 1–20, DOI: 10.1088/0953-8984/9/1/004 (1997).
6. Novoselov, K. S. *et al.* Electric field effect in atomically thin carbon films. *Science* **306**, 666–669, DOI: 10.1126/science.1102896 (2004).
7. Ferrari, A. C. *et al.* Raman spectrum of graphene and graphene layers. *Phys. Rev. Lett.* **97**, 187401, DOI: 10.1103/PhysRevLett.97.187401 (2006).
8. MacGillivray, L. R., Subramanian, S. & Zaworotko, M. J. Interwoven two- and three-dimensional coordination polymers through self-assembly of Cu' cations with linear bidentate ligands. *J. Chem. Soc., Chem. Commun.* **0**, 1325–1326, DOI: 10.1039/C39940001325 (1994).
9. Carlucci, L., Ciani, G. & Proserpio, D. M. Polycatenation, polythreading and polyknotting in coordination network chemistry. *Coord. Chem Rev.* 247–289, DOI: 10.1016/S0010-8545(03)00126-7 (2003).
10. Proserpio, D. M. Polycatenation weaves a 3d web. *Nat. Chem.* **2**, 435–436, DOI: 10.1038/nchem.674 (2010).
11. Bissell, R. A., Córdova, E., Kaifer, A. E. & Stoddart, J. F. A chemically and electrochemically switchable molecular shuttle. *Nature* **369**, 133–137, DOI: 10.1038/369133a0 (1994).
12. Fang, L. *et al.* Mechanically bonded macromolecules. *Chem. Soc. Rev.* **39**, 17–29, DOI: 10.1039/b917901a (2010).
13. v. d. Molen, S. J. *et al.* Light-controlled conductance switching of ordered metal-molecule-metal devices. *Nano Lett.* **9**, 76–80, DOI: 10.1021/nl802487j (2009).
14. Sauvage, J. P. From chemical topology to molecular machines (Nobel lecture). *Angew. Chem. Int. Ed.* **56**, 11080–11093, DOI: 10.1002/anie.201702992 (2017).
15. Dabrowski-Tumanski, P. & Sulkowska, J. I. Topological knots and links in proteins. *PNAS* **114**, 3415–3420, DOI: 10.1073/pnas.1615862114 (2017).
16. Hopf, H. Über die abbildungen der dreidimensionalen sphäre auf die kugelfläche. *Math. Annalen* **104**, 637–665, DOI: 10.1007/BF01457962 (1931).
17. Sunada, T. Lecture on topological crystallography. *Jpn. J. Math.* **7**, 1–39, DOI: 10.1007/s11537-012-1144-4 (2012).
18. Thurston, W. P. Three dimentional manifolds, Kleinian groups and hyperbolic geometry. *Bull. Amer. Math. Soc. (N.S.)* **6**, 357–381, DOI: projecteuclid.org/euclid.bams/1183548782 (1982).
19. Perelman, G. Finite extinction time for the solutions to the ricci flow on certain three-manifolds. *arXiv:math/0307245 [math.DG]* (2003).
20. Berezinskii, V. L. Destruction of long-range order in one-dimensional and two-dimensional systems having a continuous symmetry group i. classical systems. *Sov. Phys. JETP* **32**, 493–500 (1971).
21. Kosterlitz, J. M. & Thouless, D. J. Long range order and metastability in two dimensional solids and superfluids. *J. Phys. C: Solid State Phys.* **5**, L124–L126 (1972).
22. Tanda, S. *et al.* A möbius strip of single crystals. *Nature* **417**, 397–398, DOI: 10.1038/417397a (2002).
23. Kane, C. L. & Mele, E. J. z_2 topological order and the quantum spin hall effect. *Phys. Rev. Lett.* **95**, 146802, DOI: 10.1103/PhysRevLett.95.146802 (2005).
24. Hsieh, D. *et al.* A topological Dirac insulator in a quantum spin Hall phase. *Nature* **452**, 970–974, DOI: 10.1038/nature06843 (2008).
25. Ovchinnikov, A. A. & i. L. Shamovsky. The structure of the ferromagnetic phase of carbon. *J. Mol. Struct. THEOCHEM* **251**, DOI: 10.1016/0166-1280(91)85138-W (1991).

26. Kittel, C. *Introduction to Solid State Physics* (John Wiley & Sons, 2004), 8 edn.

27. Wallace, P. R. The band theory of graphite. *Phys. Rev* **71**, 622–634 (1946).

28. CastroNeto, A. H., Guinea, F., Peres, N. M. R., Novoselov, K. S. & Geim, A. K. The electronic properties of graphene. *Rev. Mod. Phys.* **81**, 109–162, DOI: 10.1103/RevModPhys.81.109 (2009).

29. Wang, Z. *et al.* Dirac semimetal and topological phase transitions in A_3Bi (A=Na, K, Rb. *Phys. Rev. B* **85**, 195320, DOI: 10.1103/PhysRevB.85.195320 (2012).

30. Liu, Z. K. *et al.* Discovery of a three-dimensional topological Dirac semimetal, Na_3Bi. *Science* **343**, 864–867, DOI: 10.1126/science.1245085 (2014).

31. Armitage, N. P., Mele, E. J. & Vishwanath, A. Weyl and Dirac semimetals in three-dimensional solids. *Rev. Mod. Phys.* **90**, DOI: 10.1103/RevModPhys.90.015001 (2018).

32. Zhu, L. *et al.* Blue phosphorene oxide: Strain-tunable quantum phase transitions and novel 2d emergent fermions. *Nano Lett.* **16**, 6548–6554, DOI: 10.1021/acs.nanolett.6b03208 (2016).

33. Bradlyn, B. *et al.* Beyond Dirac and Weyl fermions: Unconventional quasiparticles in conventional crystals. *Science* **353**, aaf5037, DOI: 10.1126/science.aaf5037 (2016).

34. Chang, G. *et al.* Nexus fermions in topological symmorphic crystalline metals. *Sci. Rep.* **7**, 1688, DOI: 10.1038/s41598-017-01523-8 (2016).

35. Lv, B. Q. *et al.* Observation of threee-component fermions in the topological semimetal molybdenum phosphide. *Nature* **546**, 627–631, DOI: 10.1038/nature22390 (2017).

36. Mermin, N. D. & Wagner, H. Absence of ferromagnetism or antiferromagnetism in one- or two-dimensional isotropic Heisenberg models. *Phys. Rev. Lett.* **17**, 1133–1136, DOI: https://doi.org/10.1103/PhysRevLett.17.1133 (1966).

37. Hohenberg, P. C. Existence of long-range order in one and two dimensions. *Phys. Rev.* **158**, 383–386, DOI: 10.1103/PhysRev.158.383 (1967).

38. Metzner, W. & Vollhardt, D. Correlated lattice fermions in $d = \infty$ dimensions. *Phys. Rev. Lett.* **62**, 324–327, DOI: 10.1103/PhysRevLett.62.324 (1989).

39. Georges, A., Kotliar, G., Krauth, W. & Rozenberg, M. J. Dynamical mean-field theory of strongly correlated fermion systems and the limit of infinite dimensions. *Rev. Mod. Phys.* **68**, 13–125, DOI: 10.1103/RevModPhys.68.13 (1996).

40. Evans, D. A. History of the Harvard ChemDraw project. *Angew. Chem. Int. Ed.* **53**, 11140–11145, DOI: 10.1002/anie.201405820 (2014).

41. Van, N. H., Muruganathan, M., Kulothungan, J. & Mizuta, H. Fabrication of a three-terminal graphene nanoelectromechanical switch using two-dimensional materials. *Nanoscale* **10**, 12349, DOI: 10.1039/c7nr08439k (2018).

42. Kim, K. S. *et al.* Large-scale pattern growth of graphene films for stretchable transparent electrodes. *Nature* **457**, 706–710, DOI: 10.1038/nature07719 (2009).

43. Segawa, Y. *et al.* Topological molecular nanocarbons: All-benzene catenane and trefoil knot. *Science* **365**, 272–276, DOI: 10.1126/science.aav5021 (2019).

44. Kaiser, K. *et al.* An sp-hybridized molecular carbon allotrope, cyclo[18]carbon. *Science* **365**, 1299–1301, DOI: 10.1126/science.aay1914 (2019).

45. Nakada, K., Fujita, M., Dresselhaus, G. & Dresselhaus, M. S. Edge state in graphene ribbons: Nanometer size effect and edge shape dependence. *Phys. Rev. B* **54**, 17954–17961 (1996).

46. Flouris, K., Jimenez, M. M. & Herrmann, H. J. Quantum spin-Hall effect on Möbius graphene ribbon. *arXiv:1902.03892 [cond-mat.mes-hall] arXiv:1902.03892 [cond-mat.mes-hall]* (2019).

47. Herges, R. Topology in chemistry: Designing möbius molecules. *Chem. Rev.* **106**, 4820–4842, DOI: 10.1021/cr0505425 (2006).

48. Chichak, K. S. *et al.* Molecular borromean rings. *Science* **304**, 1308–1312, DOI: 10.1126/science.1096914 (2004).

49. Peters, A. J., Chichak, K. S., Cantrill, S. J. & Stoddart, J. F. Nanoscale borromean links for real. *Chem. Comm.* **27**, 3394–3396, DOI: 10.1039/b505730b (2005).

50. Shirakawa, H., Louis, E. J., Macdirmid, A. G., Chiang, C. K. & Heeger, A. J. Synthesis of electrically conducting organic polymers: Halogen derivatives of polyacetylene, $(CH)_x$. *J. C. S. Chem. Comm.* 578–580, DOI: 10.1039/C39770000578 (1977).

51. Shapere, A. & Wilczek, F. Classical time crystals. *Phys. Rev. Lett.* **109**, DOI: 10.1103/PhysRevLett.109.160402 (2012).

52. Tomita, I. & Saito, S. Lattice deformation on flat-band modulation in 3d Hopf-linked carbon allotrope: Hopfene. *Appl. Phys. Lett.* **115**, DOI: 10.1063/1.5118967 (2019).

53. Saito, S. & Tomita, I. BCS-BEC crossover and superconductor-insulator transition in Hopf-linked Graphene layers: Hopfene. *Mater. Res. Express* **6**, DOI: 10.1088/2053-1591/ab4337 (2019).

54. Hebard, A. F. *et al.* Superconductivity at 18 K in potassium-doped C_{60}. *Nature* **350**, 600–601, DOI: 10.1038/350600a0 (1991).

55. Sorella, S. *et al.* Correlation-driven dimerization and topological gap opening in isotropically strained graphene. *Phys. Rev. Lett.* **121**, 066402, DOI: 10.1103/PhysRevLett.121.066402 (2018).

56. Giannozzi, P. *et al.* Quantum ESPRESSO: a modular and open-source software project for quantum simulations of materials. *J. Phys: Condens. Matter* **21**, 395502, DOI: 10.1088/0953-8984/21/39/395502 (2009).

57. Hu, J. *et al.* Three-dimensional honycomb carbon: Junction line distortion and novel emergent fermions. *Carbon* **141**, 417–426, DOI: 10.1016/j.carbon.2018.09.027 (2019).

58. Wang, B. & Ohgushi, K. Post-perovskite transition in anti-structure. *Sci. Rep.* **6**, 37896, DOI: 10.1038/srep37896 (2016).

59. Auerbach, A. *Interacting Electrons and Quantum Magnetism* (Springer, 1994).

60. Bednorz, J. G. & Müller, K. A. Possible highT_c superconductivity in the Ba-La-Cu-O system. *Z. Physik B - Condens. Matter* **64**, 189–193, DOI: 10.1007/BF01303701 (1986).

61. Giamarchi, T. *Quantum Physics in One Dimension* (Oxford University Press, 2004).

62. Weng, H., Fang, C., Fang, Z., Bernevig, B. A. & Dai, S. Weyl semimetal phase in noncetrosymmetric transition-metal monophosphides. *Phy. Rev. X* **5**, 011029, DOI: 10.1103/PhysRevX.5.011029 (2015).

63. Xu, S. Y. *et al.* Discovery of a Weyl fermion semimetal and topological Fermi arcs. *Science* **349**, 613–617, DOI: 10.1126/science.aaa9297 (2015).

64. Bardeen, J., Cooper, L. N. & Schrieffer, J. R. Theory of superconductivity. *Phys. Rev.* **108**, 1175–1204 (1957).

65. Belash, I. T., Zharikov, O. V. & Palnichenko, A. V. Superconductivity of GIC with Li, Na and K. *Synth. Met.* **34**, 455–460, DOI: 10.1016/0379-6779(89)90424-4 (1989).

66. Emery, N., Hérold, C., Marêché, J. F. & Lagrange, P. Synthesis and superconducting properties of cac6. *Sci. Technol. Adv. Mater.* **9**, 044102, DOI: 10.1088/1468-6996/9/4/044102 (2008).

67. Kamide, K., Kimura, T., Nishida, M. & Kurihara, S. Singlet superconductivity phase in carbon nanotubes. *Phys. Rev. B* **68**, 024506, DOI: 10.1103/PhysRevB.68.024506 (2003).

68. Cleuziou, J. P., Wernsdorfer, W., Bouchiat, V., Ondarçuhu, T. & Monthioux, M. Carbon nanotube superconducting quantum interference device. *Nat. Nanotech.* **1**, 53–59 (2006).

69. Bbhaumik, A., Sachan, R., Gupta, S. & Narayan, J. Discovery of high-temperature superconductivity (tc=55k) in b-doped q-carbon. *ACS NANO* **22**, 11915–11922, DOI: 10.1021/acsnano.7b06888 (2017).

70. Cao, Y. *et al.* Unconventional superconductivity in magic-angle graphene superlattices. *Nature* **556**, 43–50 (2018).

71. Micnas, R., Ranninger, J. & Robaskiewicz, S. Superconductivity in narrow-band systems with local nonretarded attractive interactions. *Rev. Mod. Phys.* **62**, 113–171 (1990).

72. Koma, A., Sunouchi, K. & Miyajima, T. Fabrication of ultrathin heterostructures with van der Waals epitacy. *J Vac Sci Technol B* **3**, DOI: 10.1116/1.583125 (1985).